Alzheimer's
Research & Therapy

RESEARCH

Open Access

Age, sex and Alzheimer's disease: a longitudinal study of 3xTg-AD mice reveals sex-specific disease trajectories and inflammatory responses mirrored in postmortem brains from Alzheimer's patients

Alicia J. Barber[1], Carmen L. del Genio[3], Anna Beth Swain[4], Elizabeth M. Pizzi[5,6], Sarah C. Watson[4], Vedant N. Tapiavala[4], George J. Zanazzi[7] and Arti B. Gaur[1,2*]

Abstract

Background Aging and sex are major risk factors for developing late-onset Alzheimer's disease. Compared to men, women experience worse neuropathological burden and cognitive decline despite living longer with the disease. Similarly, male 3xTg-AD mice, developed to model Alzheimer's disease, no longer consistently exhibit standard Alzheimer's neuropathology yet experience higher rates of mortality - providing a unique opportunity to further elucidate this dichotomy. We hypothesized that sex differences in the biological aging process yield distinct pathological and molecular Alzheimer's disease signatures in males and females, which could be harnessed for therapeutic and biomarker development.

Methods We aged male and female, 3xTg-AD and B6129 control mice across their respective lifespans ($n = 3–8$ mice per sex, strain, and age group) and longitudinally assessed neuropathological hallmarks of Alzheimer's disease, markers of hepatic inflammation, splenic mass and morphology, as well as plasma cytokine levels. We conducted RNA sequencing analysis on bulk brain tissue and examined differentially expressed genes (DEGs) between 3xTg-AD and B6129 samples and across ages in each sex. We also examined DEGs between clinical Alzheimer's and control parahippocampal gyrus brain tissue samples from the Mount Sinai Brain Bank study in each sex.

Results 3xTg-AD females significantly outlived 3xTg-AD males and exhibited progressive Alzheimer's neuropathology, while 3xTg-AD males demonstrated progressive hepatic inflammation, splenomegaly, circulating inflammatory proteins, and minimal Alzheimer's neuropathological hallmarks. Instead, 3xTg-AD males experienced an accelerated upregulation of immune-related gene expression in the brain relative to females. Our clinical investigations revealed that individuals with Alzheimer's disease develop similar sex-specific alterations in neuronal and immune function. In diseased males of both species, we observed greater upregulation of complement-related gene expression, and lipopolysaccharide was predicted as the top upstream regulator of DEGs.

*Correspondence:
Arti B. Gaur
arti.b.gaur@dartmouth.edu
Full list of author information is available at the end of the article

Conclusions Our data demonstrate that chronic inflammation and complement activation are associated with increased mortality, indicating that age-related changes in immune response contribute to sex differences in Alzheimer's disease trajectories. We provide evidence that aging and transgene-driven disease progression trigger a widespread inflammatory response in 3xTg-AD males, which mimics the impact of lipopolysaccharide stimulation despite the absence of infection.

Keywords Alzheimer's disease, 3xTg-AD mice, Sex, Age, Inflammation, RNA sequencing, Pathology

Background

Alzheimer's disease, the most common form of dementia, is a progressive neurodegenerative disorder characterized pathologically by amyloid beta (Aβ) plaques, neurofibrillary tangles (NFTs) and neuropil threads comprised of hyperphosphorylated tau, gliosis and neuroinflammation, as well as neuronal and synaptic loss [1, 2]. These neuropathological impairments create a cyclic cascade of damage, spanning a multidecade disease continuum. More than 55 million people worldwide currently have dementia, and it is expected that without effective preventative or curative therapeutic innovation, this number will reach 139 million in the year 2050 [3]. The most significant risk factor for Alzheimer's disease is age, as the likelihood of developing the disease doubles every 5 years after the age of 65 [4]. Sex differences in life expectancy thus contribute to a greater lifetime risk of dementia in women, as females outlive males by 4–7 years on average worldwide [5, 6]. However, despite their prolonged survival, even with Alzheimer's disease [7–9], women exhibit increased global Alzheimer's neuropathological burden and greater cognitive impairment [10–13]. As a result, women with Alzheimer's experience higher disability-adjusted life years due to disease compared to men [14]. The longstanding phenomenon of women presenting with higher morbidity, but lower mortality rates compared to men throughout the aging process, across diagnoses, is known as the "male–female health-survival paradox" [15, 16].

3xTg-AD mice are a widely used transgenic model to study Alzheimer's which carry *APP*, *MAPT*, and *PSEN1* gene mutations [17]. They are one of the only models to develop both Aβ plaques and NFTs, in addition to exhibiting stark sexual dimorphism [18–22]. Since the initial generation of the model, it has been described by multiple groups and confirmed by the donating investigator that male 3xTg-AD mice no longer consistently exhibit plaque and tangle pathology [23–25]. Despite this sex-specific phenotypic drift, 3xTg-AD males continue to experience higher rates of mortality relative to females [20, 21]. Marchese et al. and Kapadia et al. have provided strong evidence that 3xTg-AD mice display manifestations of systemic autoimmunity, including splenomegaly, hepatomegaly, elevated serum autoantibodies, reduced hematocrit, and elevated double-negative (CD4-/CD8-) T splenocytes, which are all exacerbated in 3xTg-AD males [26, 27]. The group proposed that this sex-dependent autoimmune mechanism may be interfering with the development of plaques and tangles in the male 3xTg-AD brain and have shown that chronic immunosuppression limits said manifestations of autoimmunity [28]. Catorce et al. further showed that 3xTg-AD mice exhibit not only sex-dependent, but also age-dependent alterations in double-negative T cell populations [29]. While these studies and others [30] have identified differences in 3xTg-AD adaptive immunity, fewer have examined sex- and age-related changes in innate immunity.

Franceschi et al. coined the term "inflammaging" to describe low-grade chronic, systemic, inflammation in aging associated with increased proinflammatory cytokine production, which is a substantial risk factor for morbidity and mortality in older adults [31]. While both sexes experience aging-associated changes in immune function [32, 33], males have been shown to experience more unfavorable changes and a greater rate of inflammaging [34, 35] or innate immune response. Inflammaging likely plays a critical role in the pathogenesis of age-related diseases [36], including Alzheimer's, influencing the manifestation of disease and survival time from diagnosis. Despite the immense impact of age and sex on Alzheimer's incidence and severity, many questions remain regarding how these leading risk factors contribute to the molecular mechanisms of Alzheimer's disease. It is especially unclear how disease trajectories, from initiation through progression of Alzheimer's, differ between males and females.

The goal of our study was to elucidate sex-specific Alzheimer's disease phenotypes that surface with age by establishing a comprehensive time course of neural and peripheral abnormalities in the 3xTg-AD mouse model. Given that aging and inflammaging affect all body systems, we looked outside of the central nervous system, examining changes in the liver, spleen, and plasma in addition to the brain. We hypothesized that sex differences in the biological aging process result in distinct disease trajectories in males and females. To test our hypothesis, we conducted a multi-year study, collecting tissues and plasma from male and female 3xTg-AD and

control mice at incremental ages across mature adult, middle age, and old age life stages. The experimental design allowed for parallel sex-specific characterization of progressive pathology and gene expression changes within "healthy" and "diseased" aging mice. Sex-specific transcriptomic profiles observed in aged 3xTg-AD mice were further substantiated in clinical Alzheimer's data, revealing clear sex differences in neuroinflammation and synaptic impairment consistent between species.

Methods

Animals

Colony Maintenance: The 3xTg-AD mice utilized were previously described [25, 26] and were obtained from The Jackson Laboratory (B6;129-Tg(APPSwe,tauP301L)1Lfa *Psen1tm1Mpm*/Mmjax; MMRRC Strain #034830-JAX). Homozygous expression for the mutations in the *PSEN1*, *APP*, and *MAPT* genes were confirmed with TaqMan Real-Time PCR assays and the colony was maintained using 3xTg-AD mice breeding pairs. Wildtype controls were bred in-house - C57BL/6J (B6; Strain #000664) females and 129S1/SvImJ males (129S; Strain #002448) were crossed to produce B6129SF1/J mice. Mice were housed 3–5 per cage, kept on a 12-h light/dark cycle, and allowed ad libitum access to food and water. All animal procedures were approved by Dartmouth College's Institutional Animal Care and Use Committee (IACUC). Blood samples obtained from sentinel mice underwent quarterly and yearly serology testing with the Multiplexed Fluorometric ImmunoAssay at Charles River Research Animal Diagnostic Services to confirm the absence of pathogens (see Supplementary Table 1, Additional file 1 for list of tested agents).

Histology

Antibodies: We obtained beta-amyloid recombinant rabbit monoclonal antibody (H31L21, catalog #700254), phospho-tau (Ser202, Thr205) mouse monoclonal antibody (AT8, catalog #MN1020), and tau mouse monoclonal antibody (HT7, catalog #MN1000) from Thermo Fisher Scientific. We obtained CD45 rabbit monoclonal antibody (D3F8Q, catalog #70257) and F4/80 XP rabbit monoclonal antibody (D2S9R, catalog #70076 from Cell Signaling Technology. *Staining*: Hemibrains, spleen, and liver tissue samples were collected from animals euthanized via carbon dioxide inhalation, followed by cervical dislocation. Transcardiac perfusion with PBS and heparin was subsequently performed. Samples were fixed in formalin for 24 h and then transferred to 70% ethanol. Tissues were stored in hinged biopsy cassettes and embedded in paraffin. Immunohistochemistry slides were cut at 4um and air dried at room temperature before baking at 60°C for 30 min. Automated protocol performed on the Leica Bond Rx included paraffin dewax, antigen retrieval and staining. Heat-induced epitope retrieval using Bond Epitope Retrieval 2, pH9 (Leica Biosystems AR9961) was incubated at 100°C for 30 min. Primary antibody was applied and incubated for 15 min at room temperature. Primary antibody binding was detected and visualized using the Leica Bond Polymer Refine Detection Kit (Leica Biosystems DS9800) with DAB chromogen and hematoxylin counterstain. *Quantification*: Slides were imaged with a 40×slide scanner and converted to digital files. QuPath software was utilized to quantify antibody staining. For Aβ staining, plaques were outlined with the QuPath wand tool, and plaque surface areas were measured and summated across the sagittal brain section. Total brain surface area, excluding the olfactory bulb and cerebellum due to variation in tissue integrity across samples, was measured. Total plaque surface area out of total brain surface area produced normalized Aβ plaque surface area values for each sample. For all other staining, QuPath automated positive cell detection analyzed the designated region of interest, generating a number of positive detections per mm^2 of annotation area. For phospho-tau staining, the subiculum and CA1 comprised the annotated region. For total tau staining, the hippocampal formation and its immediate surroundings comprised the annotated region. For CD45 and F4/80 staining, a representative portion of the liver comprised the annotated region, given the lack of anatomical differentiation. While regions of interest ranged across markers, only a single annotated region from a single brain section was quantified for each stain per individual mouse. For each batch of samples, negative controls that underwent all histology protocol steps except for primary antibody application were quantified using the same methods, and resulting values were subtracted from stained samples to normalize for background staining and technical variation.

Cytokine profiling

Plasma collection: Blood was collected retro-orbitally in living animals or through the inferior vena cava immediately following euthanasia via carbon dioxide inhalation with confirmatory cervical dislocation. This euthanasia method limited stress induced cytokine expression at the end of life and minimized differences between terminal and retro-orbital (RO) bleeds. Of the 80 total plasma samples analyzed, 25 (10 terminally bled, 15 retro-orbitally bled) came from 3xTg-AD females, 15 (7 terminal, 8 RO) came from 3xTg-AD males, 20 (9 terminal, 11 RO) came from WT females, and 20 (10 terminal, 10 RO) came from WT males. Overall, 71 individual mice were represented, with repeated blood draws only included from 9 mice. Animals were anesthetized with

isoflurane during retro-orbital bleeds. Blood samples were transferred into 1.5 mL Eppendorf tubes with edetic acid (EDTA) for anti-coagulation (4uL EDTA/ ~ 200 uL blood). Tubes were immediately placed on ice and then centrifuged at 4°C for 10 min at 1000 rcf. The supernatant was transferred to a new tube and centrifuged at 4°C for 3 min at 14,000 rpm. Plasma was transferred to a new tube and stored at -80°C until use. *Assay*: Inflammatory proteins were measured using the MILLIPLEX Mouse Cytokine/Chemokine Magnetic Bead Panel – Premixed 32 Plex – Immunology Multiplex Assay (EMD Millipore. Corporation, Billerica, MA). Calibration curves from recombinant cytokine standards were prepared with threefold dilution steps in the same matrix as the samples. High and low spikes (supernatants from stimulated PBMCs and dendritic cells) were included to determine cytokine recovery. Standards and spikes were measured in triplicate, samples were measured once, and blank values were subtracted from all readings. All assays were carried out directly in a 96-well filtration plate (Millipore, Billerica, MA) at room temperature and protected from light. Briefly, wells were pre-wet with 100 uL PBS containing 1% BSA, then beads together with a standard, sample, spikes, or blank were added in a final volume of 100 uL and incubated together at room temperature for 30 min with continuous shaking. Beads were washed three times with 100 uL PBS containing 1% BSA and 0.05% Tween 20. A cocktail of biotinylated antibodies (50 uL/well) was added to beads for a further 30-min incubation with continuous shaking. Beads were washed three times, then streptavidin-PE was added for 10 min. Beads were again washed three times and resuspended in 125 uL of PBS containing 1% BSA and 0.05% Tween 20. The fluorescence intensity of the beads was measured using the Bio-Plex array reader. Bio-Plex Manager software with five-parametric-curve fitting was used for data analysis. Intra-assay precision quality controls indicated 2.9% coefficient of variation. Data points considered out of range below (OOR <) were substituted with a 0, the minimum detectable value.

RNA isolation and sequencing

Isolation: Brain tissue was dissected from animals euthanized via carbon dioxide inhalation with confirmatory cervical dislocation, followed by perfusion with PBS and heparin. Samples were flash-frozen in liquid nitrogen and stored at -80°C. Samples were later placed in a deep-well 96-well plate with stainless steel RNase-free homogenization beads and QIAzol lysis buffer. Plates were inserted into the SPEX SamplePrep 1600 MiniG tissue homogenizer and run at maximum speed for 5 min. Following homogenization, the tissue solution was added to QIAzol lysis buffer and stored at -80°C. Lysed tissue solution was subsequently added to the QIAGEN miRNeasy Micro Kit for purification of total RNA. *Sequencing*: RNA for RNA sequencing (RNA-seq) was quantified by qubit, and integrity was measured on a fragment analyzer (Agilent). 200 ng RNA was hybridized to FastSelect probes (QIAGEN) for ribodepletion, followed by library preparation using the Kapa RNA HyperPrep kit (Roche) following the manufacturer's instructions. Libraries were pooled for sequencing on a NextSeq500 instrument (Illumina) targeting 30 M, paired-end 50 bp reads per sample. A fastqc report was generated for visual inspection of the data. Raw data were pre-processed by removing adapter sequences using Cutadapt (v3.4), aligning to the mm10 reference genome using HISAT2 (v2.1.0) and quantifying read counts using the Featurecounts function (v2.0.1) from the subreads package to generate a gene expression matrix for downstream processing. Reads mapping to rRNAs were not used for analysis and were filtered from the dataset. Pseudogenes and genes without canonical names were filtered from the matrix prior to further analysis.

RNA-Seq analysis

Batch Adjustment: To adjust for sequencing batch effects within our total sample population, ComBat-seq was applied as previously described [37]. *Differential Expression Analysis*: DESeq2 was utilized as previously described [38] to identify differentially expressed mRNAs (DEGs) between 3xTg-AD and WT controls at various ages using R (v4.3.0) and RStudio (v2023.12.0 + 369). A negative binomial generalized linear model was applied. Differential expression *p*-values were adjusted for multiple comparisons with the Benjamini-Hochberg method. *Clinical data access*: Clinical data were obtained from the Mount Sinai Brain Bank (MSBB) study through the AD Knowledge Portal [39]. Parahippocampal gyrus brain tissue samples from females with AD ($n = 103$), female controls ($n = 39$), males with AD ($n = 52$), and male controls ($n = 32$) were sequenced and analyzed. Diagnoses of AD or control (CT) were determined based on the clinical dementia rating scale, Mini Mental State Exam, and Braak staging. *Age:* In the female AD sample group, 1% were in their sixties, 8% were in their seventies, 34% were in their eighties, and 57% were in their nineties or older. In the female control group, 5% were in their sixties, 20% were in their seventies, 54% were in their eighties, and 20% were in their nineties or older. In the male AD sample group, 12% were in their sixties, 38% were in their seventies, 38% were in their eighties, and 12% were in their nineties or older. In the male control group, 25% were in their sixties, 44% were in their seventies, 13% were in their eighties, and 19% were in

their nineties or older. *Race:* The majority of individuals identified as white (91% in AD females, 80% in CT females, 88% in AD males, and 66% in CT males). The remainder were Hispanic or Black, in addition to one Asian control male. *APOE genotype:* The majority of individuals possessed no APOE4 alleles (58% in AD females, 77% in CT females, 63% in AD males, and 81% in CT males), followed by APOE4 heterozygotes (37% in AD females, 23% in CT females, 23% in AD males, and 19% in CT males), and APOE4 homozygotes (5% in AD females, 0% in CT females, 13% in AD males, and 0% in CT males). *Pathway Analysis*: Statistically significant, differentially expressed genes ($p < 0.05$) were categorized into canonical pathways using QIAGEN Ingenuity Pathway Analysis (IPA) Core Analysis [40] and Enrichr [41]. Predicted upstream regulators of DEGs were identified using IPA Upstream Analysis. *Over-Representation Analysis*: Statistically significant, differentially expressed genes ($p < 0.05$) underwent Over-Representation Analysis (ORA) to determine if specific gene ontology biological processes were likely present more than by chance. WebGestalt [42] was utilized to perform ORA with the Illumina mouseref 8 reference set. Affinity propagation was applied for redundancy reduction of enrichment categories. Differential expression *p*-values were adjusted for multiple comparisons by the Benjamini-Hochberg method.

Statistical analysis

Splenic weight, IHC markers, and cytokine concentrations were analyzed using a linear regression model with R (v4.3.0) and RStudio (v2023.12.0+369). We tested the overall effects of relevant independent variables (i.e. sex, strain, age) across samples in each analysis. Independent variables were only incorporated into a model if they were matched across all conditions (i.e. age-matched samples of each condition in splenic weight analyses). We also performed secondary linear regression analyses in which samples were organized into experimental groups (i.e. 6-month-old 3xTg-AD females). Experimental groups were then contrasted against respective control/reference groups (i.e. 6-month-old 3xTg-AD females vs. 6-month-old 3xTg-AD males). *P*-values less than 0.05 were considered statistically significant. R-squared values determined the effect size of each regression model. Effect sizes, f-statistics, and complete linear regression results can be found in Supplementary Table 3, Additional file 3. Animal survival probabilities were compared between sexes and strains using the likelihood ratio test, Wald test, and log-rank test for Kaplan-Meier analyses. A Cox proportional hazards model was used to examine the association of sex and strain with mortality risk.

Results

Multi-year longitudinal study of 3xTg-AD mice reveals sex-specific differences in life expectancy

We studied male and female 3xTg-AD mice across their lifespan and used B6129 (WT) mice as sex and age-matched controls. Brain, liver, and spleen tissues, in addition to plasma samples, were collected at successive time points starting at 3 months of age, with primary analyses being run on samples from mice aged 6-, 12-, 15-, 18-, and 21-months ($n = 3$–8 mice of each sex and strain per age group). Survival was tracked to evaluate variances in longevity between groups (Fig. 1). By the end of the study period, animals had either been sacrificed in good health for timepoint collection, sacrificed unexpectedly due to signs of imminent death (labored breathing, hunched posture, minimal movement, squinted eyes, frailty, etc.), found dead, or were still living. Data points from animals that were sacrificed for planned timepoints or still living, were censored in the survival analysis. Abnormalities observed in various organ systems during necropsy were described in Supplementary Table 2, Additional file 2, however, it is unknown if manifestations were directly related to disease progression, and most animals found dead were not dissected due to their state of decomposition.

3xTg-AD mutations were associated with a substantially increased risk of mortality, as 3xTg-AD mice had nearly 100 times the risk of mortality than controls (hazard ratio 95.2, 95% confidence interval 22.33–405.71, Table 1). WT mice experienced no natural mortality events up to 2-years of age (730 days), with animals surviving past 30 months. Compared to their respective controls, male 3xTg-AD life expectancy was 12 months shorter on average, while female 3xTg-AD life expectancy was 6 months shorter on average. 3xTg-AD male mice largely did not survive past 18 months of age, while 3xTg-AD females exhibited lifespans up to roughly 24 months. Male sex was associated with an increased risk of mortality, with a hazard ratio of 2.75 (95% confidence interval 1.79–4.22, Table 1). Overall, our results demonstrate that the 3xTg-AD mice have a significantly shortened lifespan, which is further exacerbated in male mice.

Sex-specific severity of hallmark Alzheimer's neuropathology

To characterize the initiation and progression of Alzheimer's-related neuropathology, longitudinal immunohistochemistry analyses were run on sagittally-cut brain hemispheres in female and male 6-, 12-, 15-, 18-, and 21-month-old (oldest age dependent upon survival) ($n = 3$–8 mice of each sex per age group) 3xTg-AD mice. Wild-type mice do not naturally develop Aβ plaques and NFTs [43–45], therefore B6129 mice were not included

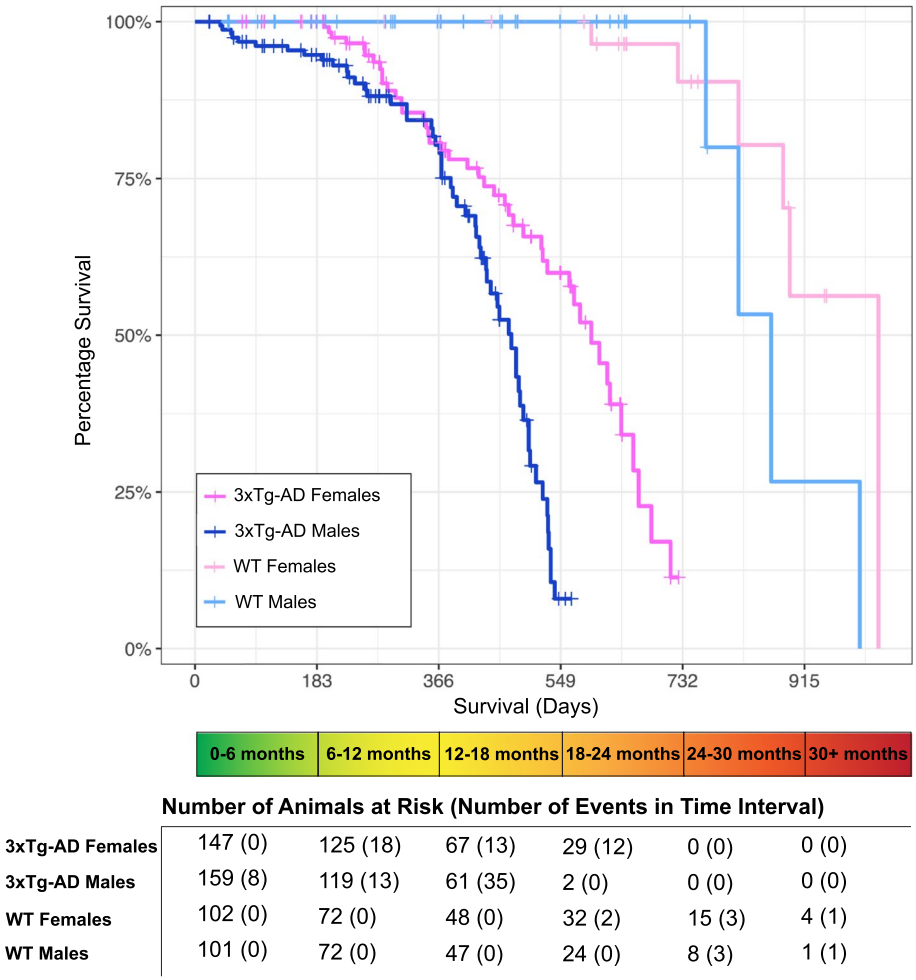

Fig. 1 3xTg-AD females outlive males. Kaplan-Meier curves for the survival of animals by sex and strain (3xTg-AD and B6129 (WT)). Data were available for 509 mice. Planned mortality events for timepoint sample collection were censored (+). Uncensored mortality events included animals that were found dead or sacrificed due to observed signs of imminent death. The number of animals at risk and the number of uncensored mortality events per 6-month time interval are shown below the graph

Table 1 Multivariate Cox regression analysis of animal survival

Characteristics	Hazard Ratio	95% Confidence Interval	*P*-value
Sex (male)	2.72	1.79–4.22	3.81E-16
Strain (3xTg-AD)	95.2	22.33–405.71	7.34E-10

The likelihood ratio test, Wald test, and log-rank test were all significant ($p < 2E\text{-}16$). $n = 509$ mice, number of events = 109

in these analyses. Characteristic hallmarks of Alzheimer's neuropathology, Aβ plaques, NFTs, and total tau expression were analyzed. Aβ antibody (H31L2) staining of brain samples was used to evaluate plaque accumulation throughout the course of the disease. We observed that extracellular Aβ plaques were first detectable at 12-months-old in the hippocampal formation of female 3xTg-AD mice, and plaque accumulation progressed significantly with age (Fig. 2a). By 15 months of age, plaques were also observed in the female 3xTg-AD pons, anterior olfactory nucleus, and cerebral cortex. Extracellular Aβ plaques were not detected in any male 3xTg-AD brain samples across the lifespan. Representative images of 18-month-old female and male 3xTg-AD hippocampal sections revealed a cluster of Aβ plaques in the female subiculum; however, the male brain does not present with plaque deposition (Fig. 2b). These results indicate that female 3xTg-AD mice exhibit an age-dependent accumulation of Aβ plaques. Further, Aβ protein aggregation is specific to females in the 3xTg-AD model, and plaque pathology is not contributing to the shortened lifespan of 3xTg-AD males.

To assess the accumulation of NFTs during the course of the disease, sagittally cut brain hemispheres were

collected from female and male 6-, 12-, 15-, 18-, and 21-month-old 3xTg-AD mice (oldest age dependent upon survival) ($n=3$–8 mice of each sex per age group) and stained with a phospho-tau (Ser202, Thr205) antibody (AT8). NFTs and neuropil threads were quantified within the CA1 and subiculum. We observed that phospho-tau pathology started in 15-month-old 3xTg-AD female mice and progressed significantly with age (Fig. 2c). Slight tangle pathology was observed in 3xTg-AD male mice, with very minimal levels of accumulation measured at 18 months of age. Representative images of 18-month-old female and male 3xTg-AD hippocampal sections reveal a significantly higher density of tangles in the female subiculum compared to the male subiculum (Fig. 2d). Comparable analyses were conducted with a tau antibody (HT7) to measure levels of total tau expression ($n=5$–8 mice of each sex per age group). Tau-positive cells were quantified within a chosen region including and surrounding the hippocampal formation. We found that tau expression progressed with age, more significantly in 3xTg-AD females compared to males (Fig. 2e). Representative images of 18-month-old female and male 3xTg-AD hippocampal sections revealed a greater density of tau-positive cells in the female entorhinal cortex compared to the male entorhinal cortex (Fig. 2f). These results indicate that phospho-tau and total tau are significantly higher in the brains of 3xTg-AD female mice compared to males.

Male 3xTg-AD mice demonstrate severe splenic and hepatic inflammation

To investigate the impact of disease progression outside of the central nervous system, we assessed spleen and liver histology. We measured splenic weight in 6- and 18-month-old, male and female, 3xTg-AD and WT mice ($n=4$–6 mice of each sex and strain per age group). 3xTg-AD male mice exhibited significantly enlarged spleens, with an average weight of 4.6 g in 18-month-old 3xTg-AD male mice, 36× the size of age-matched control spleens, and nearly 15% of their total body weight (Fig. 3a). Additionally, hematoxylin and eosin staining revealed histological changes in 3xTg-AD male splenic tissue, with a relative decrease in white pulp. As splenomegaly developed, the pink vascular spaces of the spleen and lymphoid follicles were encroached upon by infiltrating neutrophils [46]. This results in the obstruction of venous outflow of blood and abnormal enlargement in size. Representative images of spleens from 18-month-old, female and male, 3xTg-AD and WT mice (Fig. 3b) captured these changes. Overall, these results suggest that 3xTg-AD male mice experience immense splenomegaly, possibly as a result of peripheral organ inflammation, at the end of their lives.

To elucidate a potential source of peripheral organ dysfunction that could be contributing to splenomegaly, we measured two markers of inflammation in liver tissue throughout the course of disease progression. Liver tissue was collected from 6-, 12-, 15-, 18-, and 21-month-old male and female, 3xTg-AD and WT mice (oldest age dependent upon survival) ($n=3$–5 mice of each sex and strain per age group). Liver tissue was stained with a CD45 antibody to evaluate tissue wide inflammation. CD45 antigen, or leukocyte common antigen, is expressed on almost all hematopoietic cells except for mature erythrocytes [47]. We found that CD45 levels were significantly elevated in 3xTg-AD males compared to controls, as early as 6 months of age, while levels were not significantly elevated in 3xTg-AD females compared to controls until 21 months of age (Fig. 3c, d). To detect inflammation specifically resulting from increased macrophage infiltration, liver tissue was stained with F4/80, a marker for Kupffer cells—liver-specific macrophages. F4/80 levels were significantly elevated in 3xTg-AD males compared to controls, beginning at 12 months of age (Fig. 3e). However, in 3xTg-AD females a significant increase in macrophage infiltrates compared to controls was not observed until 21 months of age (Fig. 3e, f). Overall, these results indicate that 3xTg-AD males exhibit prolonged hepatic inflammation, which is present

(See figure on next page.)

Fig. 2 3xTg-AD females exhibit progressive Alzheimer's disease neuropathology. **A** Quantitative analysis of Aβ plaque deposition across sagittal brain sections in female and male 3xTg-AD mice at 6-, 12-, 15-, 18-, and 21-months-old. **B** Representative images of hippocampal sections from 18-month-old female and male 3xTg-AD mice stained with a beta- amyloid-specific antibody ($n=3$–8/sex + age). Red squares highlight regions with differences in immunoreactivity between sexes. **C** Quantitative analysis of phosphorylated-tau (Ser202, Thr 205) positivity in the CA1 and subiculum of female and male 3xTg-AD mice at 6-, 12-, 15-, 18-, and 21-months-old. **D** Representative images of hippocampal sections from 18-month-old female and male 3xTg-AD mice stained with a phosphorylated-tau-specific antibody ($n=3$- 8/sex + age). Red squares highlight regions with differences in immunoreactivity between sexes. **E** Quantitative analysis of total tau positivity surrounding the hippocampus of female and male 3xTg-AD mice at 6-, 12-, 15-, 18-, and 21-months-old. **F** Representative images of hippocampal sections from 18-month-old female and male 3xTg-AD mice stained with a tau- specific antibody ($n=5$–8/sex + age). Red squares highlight regions with differences in immunoreactivity between sexes. Data were analyzed with a linear regression model (see extended results in Supplementary Table 3, Additional file 3). Asterisks indicate significant differences between compared groups (* = $p<0.05$, ** = $p\le0.01$, *** = $p\le0.001$, **** = $p\le0.0001$). Error bars represent mean with SD

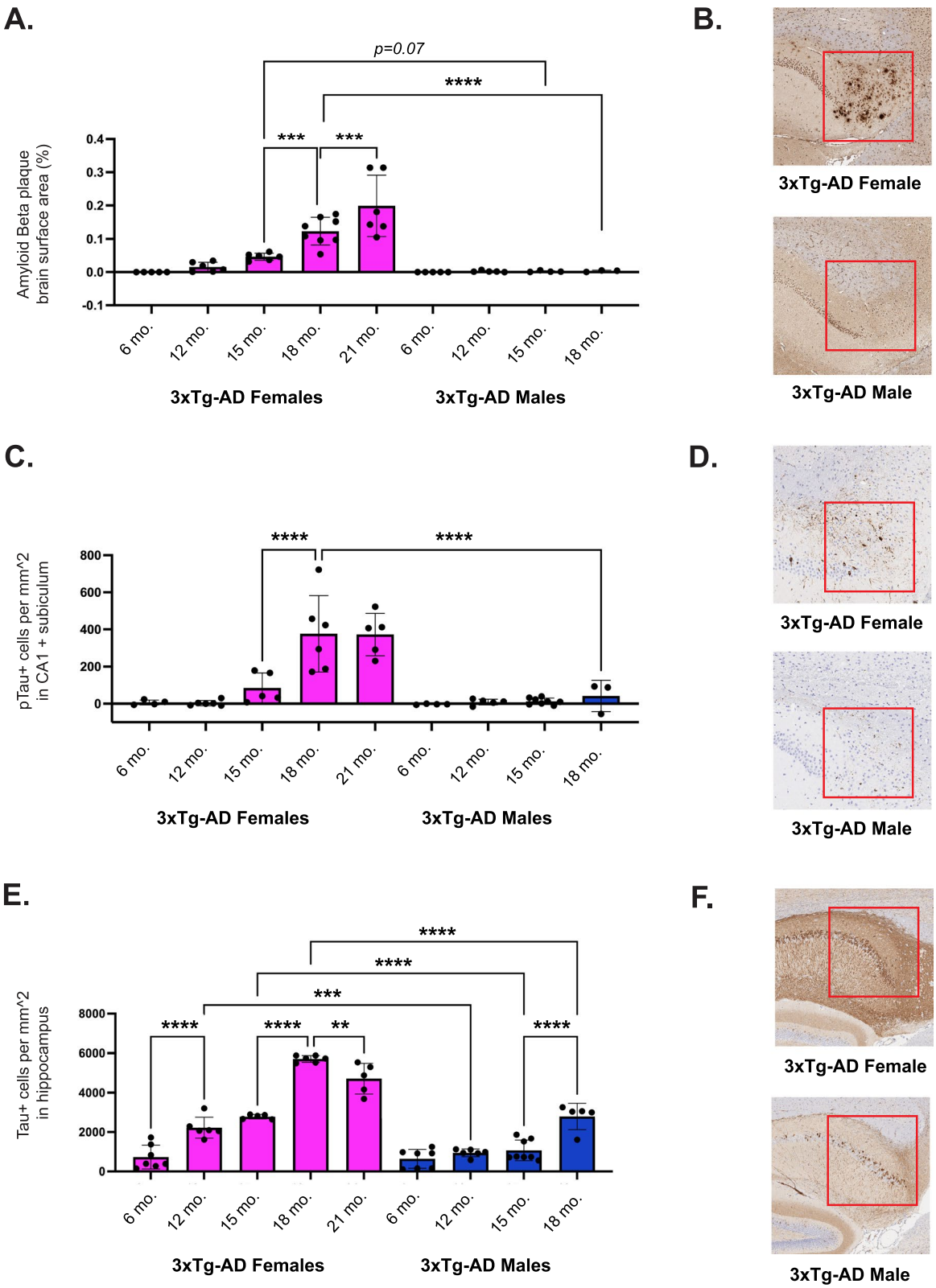

Fig. 2 (See legend on previous page.)

at 6 months of age and persists throughout the lifespan, likely contributing to splenomegaly and heightened mortality.

Aged 3xTg-AD mice exhibit sex-specific plasma cytokine profiles

To investigate the systemic impact of aging and disease progression, we measured the concentrations of cytokines, chemokines, and growth factors in the plasma of male and female, 3xTg-AD and control mice, at 6-, 15-, 18-, 21-, and 24-months-old (oldest age dependent upon survival) ($n=3$–6 mice of each sex and strain per age group). We found that levels of interleukin (IL)-12, IL-10, IL-6, and CXC chemokine ligand (CXCL) 2 were significantly increased in 3xTg-AD males only, at 18 months of age, while CXCL9 and CXCL10 levels were significantly increased in 3xTg-AD females only, at 24 months of age (see Supplementary Fig. 1, Additional file 4). Further, CC chemokine ligand (CCL) 4, CXCL1, and granulocyte-colony stimulating factor (G-CSF) levels were significantly increased in 3xTg-AD males at 15 months of age and trended upward in 3xTg-AD females, nearing statistical significance between 21 and 24 months of age. Overall, these results indicate that 3xTg-AD males exhibit exacerbated systemic inflammation relative to 3xTg-AD females, with more inflammatory proteins circulating in their bloodstream in late-stage disease progression and old age.

3xTg-AD mice manifest sex-specific timelines of immune-related gene expression in the brain

Transcriptomic profiling of female and male 3xTg-AD and WT brains was carried out across their lifespans to investigate potential molecular changes in the brain associated with the described neuropathology and systemic inflammation observed during the course of disease progression. RNA-Seq was performed on bulk brain tissue from animals between the ages of 6 and 24-months-old, depending on lifespan ($n=3$–4 mice of each sex and strain per age group) (see exploratory analysis of total sample population in Supplementary Fig. 2, Additional file 5). Mice are considered mature adults from about 3–6 months of age. However, at about 3-months-old mice are just finishing a period of puberty, rapid aging, and maturational growth and are equivalent to about 20-years-old in human years. At 6-months-old, mice are equivalent to about 30-years-old in human years and will begin experiencing age-related changes past this point [48, 49]. For these reasons, 6 months old was chosen as the mature adult baseline for comparisons in differential gene expression. A negative binomial generalized linear model was utilized to measure genes differentially expressed at progressive ages compared to a baseline of 6-months-old (see all significant DEGs in Supplementary Table 4, Additional file 6). We found that in 3xTg-AD females and males, numerous genes were increasingly dysregulated with age, exhibiting peak differential expression at the oldest time points (Fig. 4a, b).

To understand the foremost biological implications of these molecular changes, we performed overrepresentation analyses on each set of differentially expressed genes, revealing the most enriched Gene Ontology (GO) biological processes over time (Fig. 4c). Additionally, we performed Enrichr pathway analyses on each set of differentially expressed genes, to establish altered pathways over time (see all significant pathways in Supplementary Table 5, Additional file 7, and Supplementary Table 6, Additional file 8). Our analyses demonstrated that for both 3xTg-AD females and males, the majority of enriched biological processes were related to immune regulation; however, the initial age at which significant dysregulation of these processes became evident differed between sexes (Fig. 4c). Beginning at 12-months-old, 3xTg-AD males had enriched complement system activation gene expression in their brains, relative to their 6-month-old baseline. Additional immune-related biological processes were enriched at 15 and 18 months of age, such as immunoglobulin (Ig)-mediated immune response, which included greater numbers of total differentially expressed genes. Contrary to the dysregulation in males that started at 12 months, significantly enriched biological processes were not evident in 3xTg-AD female mice until 18 months of age, relative to their 6-month-old

(See figure on next page.)

Fig. 3 3xTg-AD males experience exacerbated age-dependent peripheral inflammation. **A** Splenic weight of female and male, 3xTg-AD and WT mice at 6-, and 18-months-old ($n=4$- 6/sex + age). **B** Representative hematoxylin and eosin staining of spleen tissue in 18-month-old female and male, 3xTg-AD and WT mice depicting differences in white pulp organization. **C** Quantitative analysis of CD45 positivity in liver tissue from female and male 3xTg-AD mice at 6-, 12-, 15-, 18-, and 21-months-old. **D** Representative images of liver tissue from 18-month-old female and male, 3xTg-AD and wildtype mice, stained with a CD45-specific antibody ($n=3$- 7/sex + age). **E** Quantitative analysis of F4/80 positivity in liver tissue from female and male, 3xTg-AD and WT mice at 6-, 12-, 15-, 18-, and 21-months-old. **F** Representative images of liver tissue from 18-month-old female and male, 3xTg-AD and WT mice, stained with an F4/80- specific antibody ($n=3$–6/sex + age). Data were analyzed with a linear regression model (see extended results in Supplementary Table 3, Additional file 3). Asterisks indicate significant differences between compared groups (* = $p<0.05$, ** = $p\leq0.01$, *** = $p\leq0.001$, **** = $p\leq0.0001$). Error bars represent mean with SD

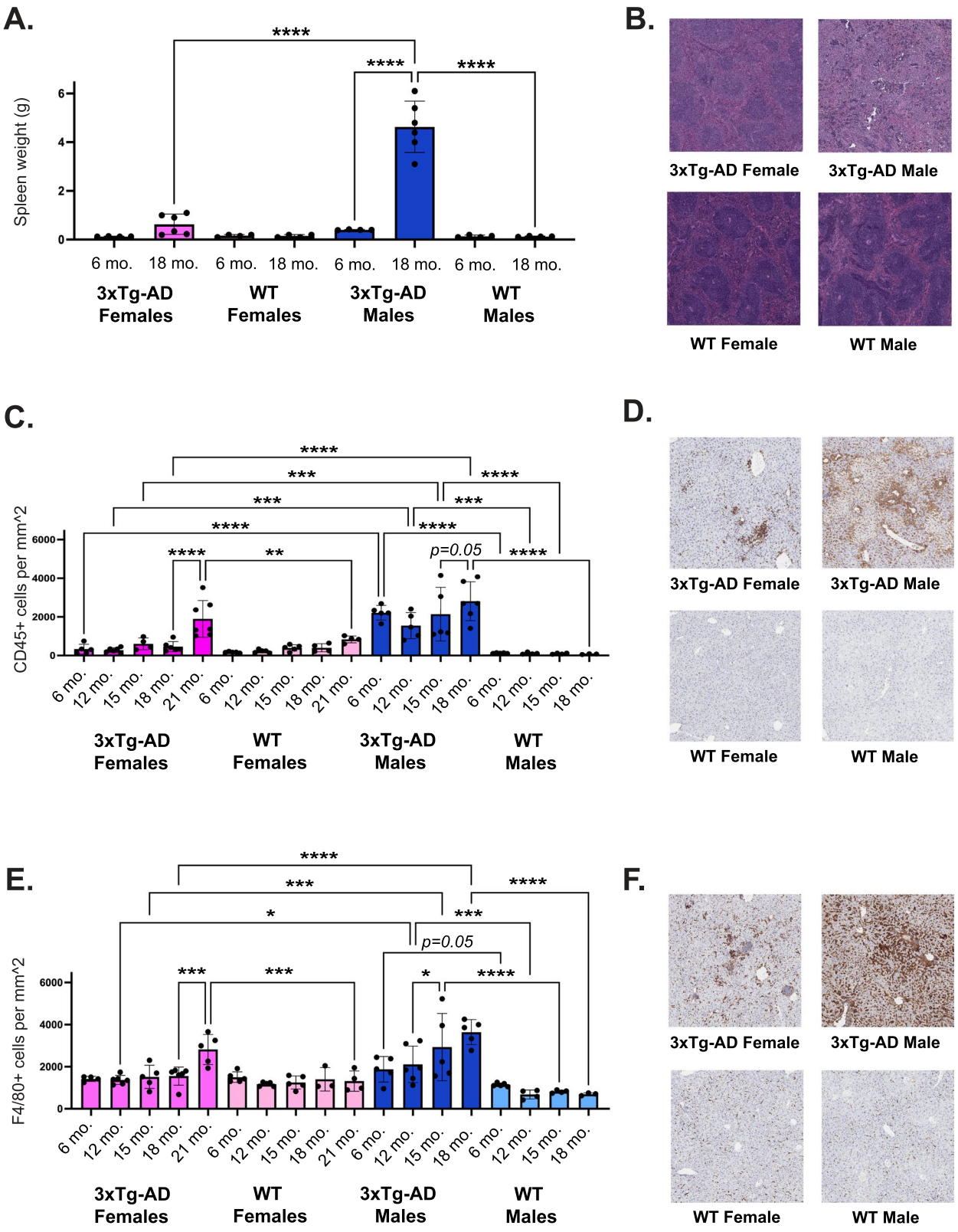

Fig. 3 (See legend on previous page.)

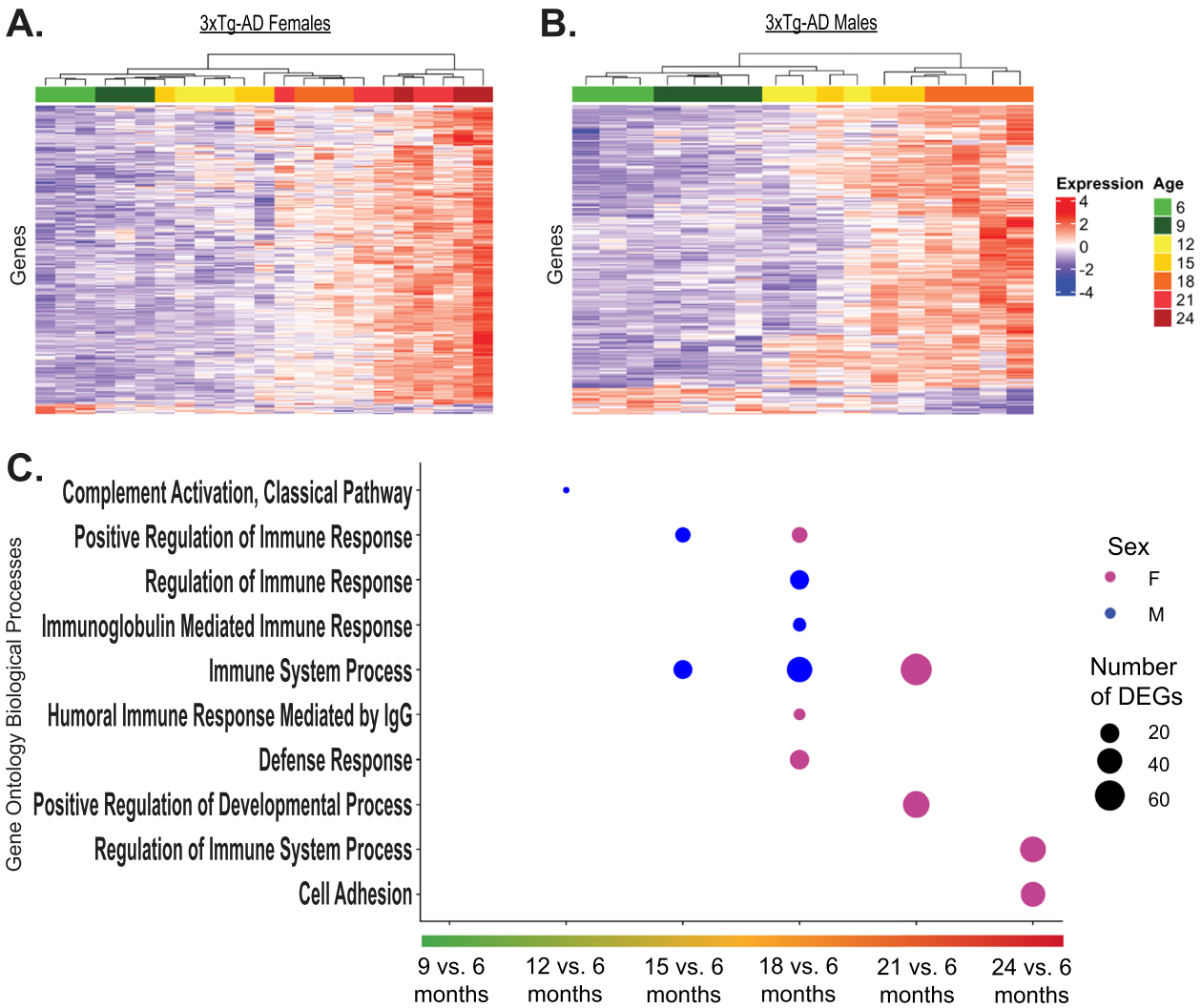

Fig. 4 3xTg-AD males exhibit accelerated age-dependent upregulation of immune- related genes in the brain. Total RNA was isolated from the bulk brain tissue of female and male, 6–24-month-old (oldest age dependent upon survival), 3xTg-AD mice and sequenced. Longitudinal differential expression analyses were performed, measuring differences in gene expression of subsequent ages compared to a baseline of 6-months-old ($n = 3$–4/sex + age) with a negative binomial generalized linear model. **A** Heatmap of genes with differential expression in 3xTg-AD females over the course of disease progression (padj < 0.05). Each column represents an individual animal, and age at time of collection is indicated by color. Samples range from 6–24 months of age. **B** Heatmap of genes with differential expression in 3xTg-AD males over the course of disease progression (padj < 0.05). Each column represents an individual animal, and age at time of collection is indicated by color. Samples range from 6–18 months of age. **C** Overrepresentation analysis of significant DEGs between various ages and a 6-month-old baseline. Affinity propagated, overrepresented Gene Ontology biological processes are plotted for females in pink and males in blue. Data were analyzed by one-tailed Fisher's Exact test. *P*-values were adjusted for multiple comparisons via Benjamini-Hochberg correction. Number of DEGs indicates number of significant differentially expressed genes from dataset driving enrichment of biological processes

baseline, including humoral immune response mediated by IgG and defense response. Additional immune-related biological processes were further enriched at 21- and 24-months-old. Corresponding analyses were conducted in female and male control mice, revealing minimal molecular changes spanning the ages of 6- to 21-months-old (see Supplementary Fig. 3, Additional file 9). These results indicate that the brains of 3xTg-AD mice exhibit highly modulated transcriptomic profiles that worsened with age and can be largely characterized by an upregulation of immune-related processes. Further, 3xTg-AD male mice exhibit accelerated upregulation of immune-related gene expression over the course of disease progression, presenting with

significant molecular dysfunction 6-months prior to 3xTg-AD females.

Aged 3xTg-AD mice and Alzheimer's patient brains exhibit sex-specific molecular profiles

To determine how the transcriptomic profiles of aged female and male 3xTg-AD brains directly differ from non-diseased controls, we conducted differential expression analyses in 15 and 18-month-old mice ($n=6$ mice of each sex and strain) (see visualization of DEGs in Supplementary Fig. 4, Additional file 10; see all significant DEGs in Supplementary Table 7, Additional file 11). We found that the resulting statistically significant DEGs could be broken down into three categories: (1) genes that were exclusively differentially expressed in 3xTg-AD females compared to controls, (2) genes that were differentially expressed in both 3xTg-AD females and males compared to controls, or (3) genes that were exclusively differentially expressed in 3xTg-AD males compared to controls. To characterize these sex-specific and overlapping sets of genes, we performed overrepresentation analyses, revealing the most enriched Gene Ontology biological processes in each category (Fig. 5a). Female-specific DEGs were primarily associated with synaptic function, overlapping DEGs were most associated with immune response, and male-specific DEGs were largely associated with additional immune-related processes. To understand further the specific biological pathways of these molecular changes, we performed IPA Core Analysis on significant DEGs. The top 12 altered canonical pathways are plotted for females (Fig. 5c) and males (Fig. 5e) (see all significant pathways in Supplementary Table 8, Additional file 12). Our analyses indicate that many immune-related pathways, including pathogen-induced cytokine storm signaling and phagosome formation, were dysregulated in 3xTg-AD male mice. In contrast, in 3xTg-AD female mice, various neural signaling pathways were dysregulated including serotonin receptor signaling, dopamine feedback in cAMP signaling, and GPCR signaling. Interestingly, the complement system was altered in both female and male 3xTg-AD mice, with the highest ratio of differentially expressed genes.

To validate our transcriptomic findings' relevance and translational impact in 3xTg-AD mice, we sought to determine how and if the observed sex-specific molecular profiles in our animal model compared to Alzheimer's disease-related changes in human brains. We examined DEGs in the parahippocampal gyrus (PHG) of males ($n=52$) and females ($n=103$) with Alzheimer's disease compared to sex and age-matched (60–90 + years-old) non-demented controls ($n=32$ males, $n=39$ females), obtained from the Mount Sinai Brain Bank (MSBB) study [43]. The PHG has been shown to carry the strongest molecular signal of late-onset Alzheimer's disease [50]. Again, within the total population of highly significant DEGs, some genes were specifically altered in one sex, while others were differentially expressed in both sexes. When performing overrepresentation analyses on sex-specific and overlapping sets of genes, the same molecular signatures found in 3xTg-AD mice were observed, as female-specific DEGs were most involved in synaptic function, overlapping DEGs were most associated with immune system process and male-specific DEGs were further associated with the immune system (Fig. 5b). Similarly, IPA Core Analysis revealed altered glutaminergic receptor signaling, synaptogenesis signaling, and axonal guidance signaling pathways in female Alzheimer's brains (Fig. 5d), while pathways like neutrophil extracellular trap signaling and neuroinflammation signaling were altered in male Alzheimer's brains (Fig. 5f) (see all significant pathways in Supplementary Table 8, Additional file 12). These results indicate that both female 3xTg-AD mice and females with Alzheimer's exhibit a sex-specific molecular phenotype related to

(See figure on next page.)

Fig. 5 Both aged 3xTg-AD mice and clinical Alzheimer's disease brains exhibit sex- specific molecular profiles. **A** Total RNA was isolated from the bulk brain tissue of 15–18- month-old, female and male, 3xTg-AD and WT mice, and sequenced. Differential expression analyses were performed between female 3xTg-AD and WT mice ($n=6$ 3xTg-AD, 6 WT) as well as between male 3xTg-AD and WT mice ($n=6$ 3xTg-AD, 6 WT) with a negative binomial generalized linear model. ORA of sex-specific and sex-overlapping significant DEGs (padj < 0.05) in 3xTg-AD mice vs. WT is depicted. Enrichment ratios of significant (FDR < 0.05), affinity propagated, overrepresented GO biological processes, are plotted for female-specific genes in pink, sex-overlapping genes in purple, and male-specific genes in blue. Data were analyzed by one-tailed Fisher's Exact test. *P*-values were adjusted for multiple comparisons via Benjamini-Hochberg correction. Significance is indicated with asterisks (** = $p \leq 0.01$, **** = $p \leq 0.0001$). **B** DEGs in the PHG of females with AD vs. controls (CT) ($n=103$ AD, 39 CT) as well as males with AD vs. controls ($n=52$ AD, 32 CT) were analyzed. ORA of significant DEGs (padj < 0.001) in individuals with AD compared to controls is depicted. Further details described previously. Top 12 significantly altered canonical pathways in **C** the brains of female 15–18-month-old 3xTg-AD vs. WT, **D** the PHG of females with AD vs. CT, **E** the brains of male 15–18-month-old 3xTg-AD vs. WT, and **F** the PHG of males with AD vs. CT. **C**-**F** Number of DEGs indicates sum of significant DEGs in dataset driving predicted pathway alteration. Gene ratio indicates number of DEGs out of total genes associated with a specific pathway. Values greater than 1.3 [-log(0.05)] are significant. **G** Complement system gene expression in the brains of 15–18-month-old female and male 3xTg-AD vs. WT, and **H** in the PHG of females and males with AD vs. CT. Log2FC = Log2 fold change

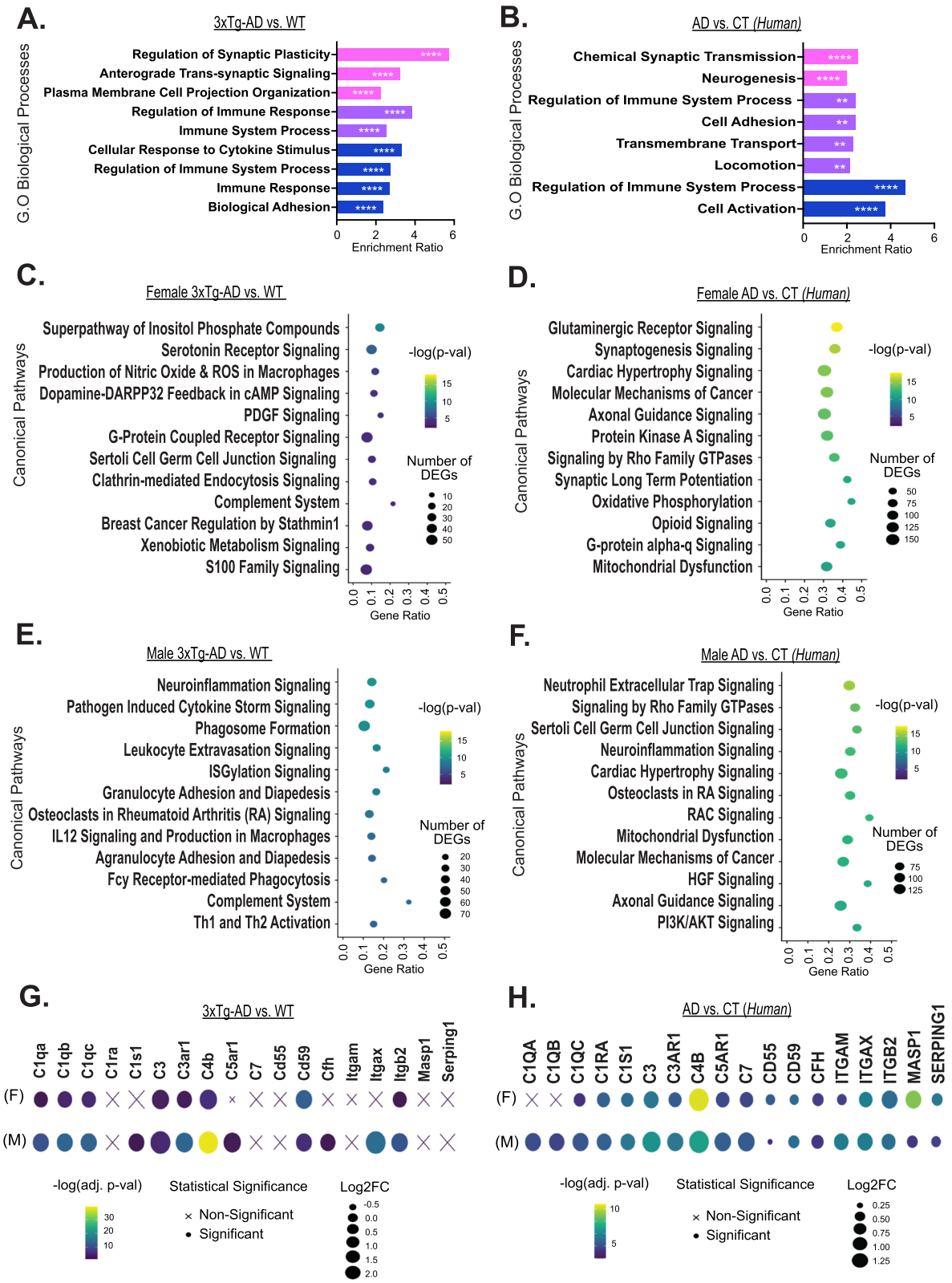

Fig. 5 (See legend on previous page.)

neuronal function, while male 3xTg-AD mice and males with Alzheimer's exhibit an exacerbated neuroinflammatory molecular phenotype.

Overexpression of complement system genes found in 3xTg-AD mouse and Alzheimer's patient brains

To dig deeper into the involvement of the complement system in Alzheimer's disease, we examined the expression of specific complement-related genes. In the brains of 3xTg-AD mice, upregulation of complement-related DEGs including *C1q* and *C4b* indicated that the classical complement pathway was activated (Fig. 5g). All complement-related DEGs had greater log-fold change and more statistical significance in 3xTg-AD males compared to females, and select genes including *C1s1, C5ar1, Cfh,* and *Itgax* only reached statistical significance in males. In the parahippocampal gyrus of humans with Alzheimer's disease, activation of the classical complement pathway was also revealed; however, further sex differences were observed as *C1QA, C1QB,* and *C1QC* reached statistical significance in males while only *C1QC* reached statistical significance in females (Fig. 5h). Similar to the observations made in 3xTg-AD mice, the majority of complement-related DEGs had greater log-fold change and more statistical significance in males compared to females. However, a few genes were more enriched in females, including *CD55* and *SERPING1*, which both function as complement inhibitors. Another gene with stronger differential expression in females was *MASP1*, activated by the lectin complement pathway which is initiated by the binding of mannose-binding lectin to bacterial surfaces with mannose-containing polysaccharides [51]. This likely also explains the greater statistical significance of *C4B* in females relative to males, as C4 is involved in classical and lectin activation pathways. Overall, our results further substantiate the involvement of complement system activation in Alzheimer's disease and suggest that sex likely impacts the severity of complement overactivation, with males exhibiting increased upregulation of most complement DEGs, and reduced expression of complement inhibitors, relative to females.

Alzheimer's-associated immune cascade resembles downstream effects of LPS stimulation

Based on the abnormal gene expression patterns in female and male Alzheimer's brains, we used IPA to predict which upstream regulators are likely driving Alzheimer's-associated differential expression and pathogenesis (see Supplementary Table 9, Additional file 13). The top 5 predicted upstream regulators are plotted for females (Fig. 6a, b) and males (Fig. 6c, d). In the mouse and human datasets, we see *MAPT* and *APP* as top predicted upstream regulators, which is to be expected given the animal model and disease pathology. However, a striking stand out is that lipopolysaccharide (LPS), an outer-membrane component of gram-negative bacteria and an intense stimulator of the innate immune system, is the number 1 top predicted upstream regulator of gene expression changes in mouse and human male brains. Extensive serology and parasitology analyses have confirmed the absence of pathogens in our utilized animal facility throughout the course of this study (see Supplementary Table 1, Additional file 1 for list of tested agents). Hence, we propose a model in which the Alzheimer's-associated immune response, clearly exacerbated in males, resembles the downstream effects of LPS stimulation (Fig. 6e). Based on our findings, we hypothesize that mutations in *APP, MAPT,* and *PSEN1* genes yield a compounding effect with age, triggering biological changes which initiate an inflammatory response that mimics the effects of LPS stimulation, despite the absence of infection. Neural activation of additional inflammatory factors, and well-known drivers of inflammaging, including IL-1β, IL-6, TNF, and IFNγ, were also predicted. This process prompts the sustained upregulation of complement system genes, possibly contributing to observed systemic inflammation, hepatic inflammation, and splenomegaly, driving increased mortality. Conversely, these chronic inflammatory forces are likely preventing the aggregation of AD-associated proteins in the brains of 3xTg-AD males.

(See figure on next page.)

Fig. 6 Alzheimer's disease-associated immune cascade, exacerbated in males, resembles downstream effects of lipopolysaccharide stimulation in mice. Top 5 predicted upstream regulators of DEGs in **A** female 3xTg-AD mouse brains compared to WT ($n = 6$ 3xTg-AD, 6 WT), **B** female Alzheimer's disease (AD) parahippocampal gyrus (PHG) compared to controls (CT) ($n = 103$ AD, 39 CT), **C** male 3xTg-AD mouse brains compared to WT ($n = 6$ 3xTg-AD, 6 WT), and **D** male AD PHG compared to CT ($n = 52$ AD, 32 CT). **E** Proposed model of disease pathogenesis in 3xTg-AD males. Overexpressed transgenes are translated in the central nervous system. Aging and disease progression triggers inflammatory response, mimicking effects of LPS stimulation, despite absence of infection. Complement system is activated and associated genes are upregulated. Aβ plaque and NFT formation is prevented. Liver is chronically inflamed, resulting in the development of splenomegaly. Inflammatory cytokines circulate in the bloodstream. *Created with BioRender.com*

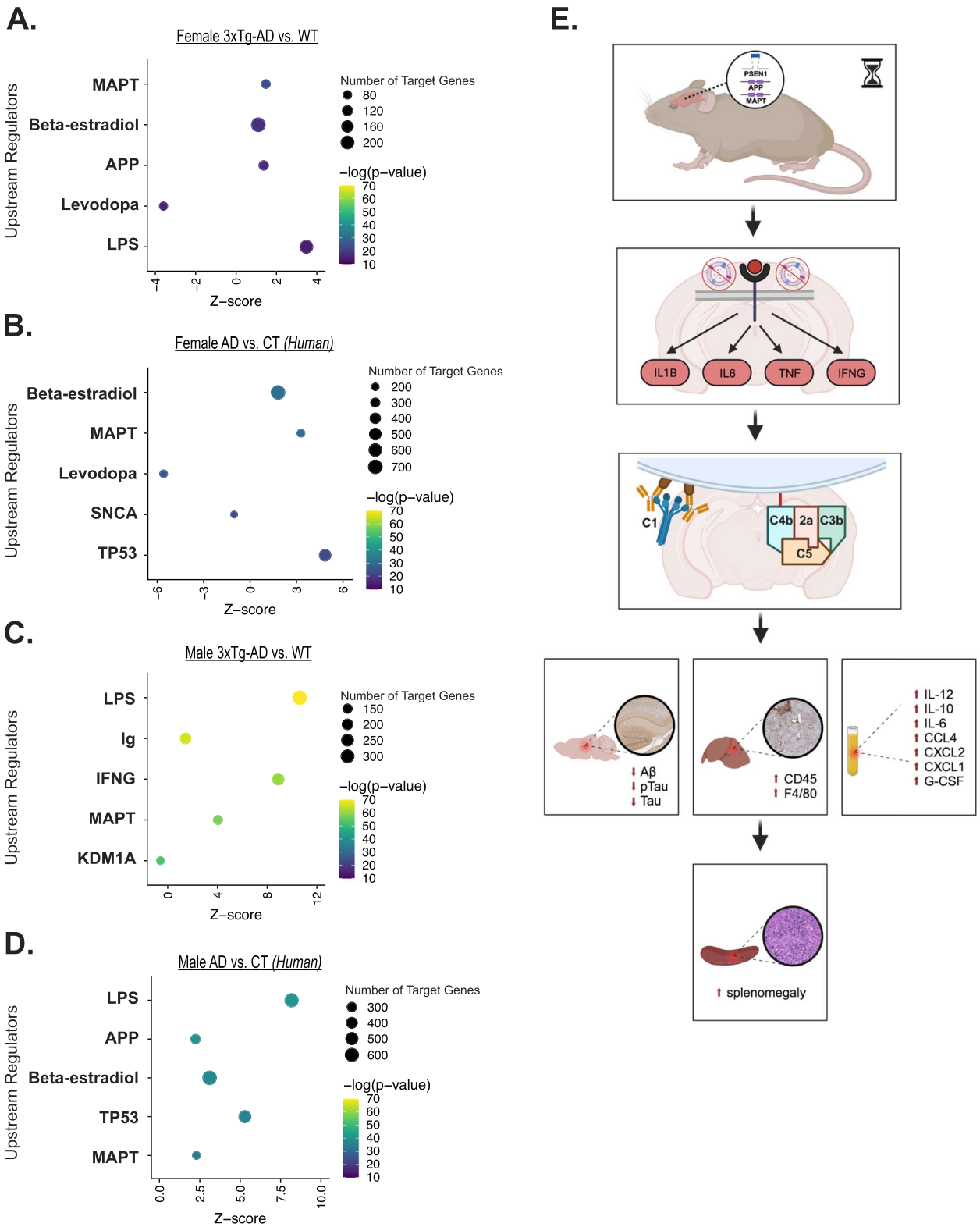

Fig. 6 (See legend on previous page.)

Discussion

It remains unclear how and when sex differences in biological aging emerge and contribute to Alzheimer's disease pathogenesis. We hypothesized that aging differentially affects biological processes in males and females, resulting in distinct trajectories of disease. In this study, we first reproduced and then expanded upon previously reported findings in the 3xTg-AD mouse model. Throughout the course of our 30-month investigation, we recorded all deaths, revealing significantly greater longevity in 3xTg-AD females compared to males (Fig. 1). We also quantified Alzheimer's related neuropathology in the brains of female and male 3xTg-AD mice across adulthood (Fig. 2), providing additional evidence that 3xTg-AD females exhibit progressive Alzheimer's hallmark pathologies. In contrast, 3xTg-AD males exhibit no Aβ plaque pathology and very minimal tangle pathology, if any, in old age. Additionally, we showed that severe splenomegaly was present in aged 3xTg-AD males and associated with abnormal histology (Fig. 3a, b). Together, these results align with published literature [20, 21, 23, 24, 26, 27] and reinforce the translatability of the 3xTg-AD model.

To build upon this foundational evidence, we conducted a longitudinal analysis of liver inflammation in female and male 3xTg-AD and control mice. Hepatomegaly has been previously reported in the 3xTg-AD model [26, 27, 52], however, we have expanded upon this knowledge by exploring hepatocellular expression of CD45 and F4/80 across sex, age, and disease status. We discovered that male 3xTg-AD mice exhibit significant chronic hepatic inflammation throughout adulthood, while females exhibit milder hepatic inflammation in old age (Fig. 3c-f). These results help to elucidate a potential driver of splenomegaly in male 3xTg-AD mice, as liver diseases such as cirrhosis and hepatitis are one of the most common causes of splenomegaly clinically [53]. Additionally, our results raise further questions regarding the involvement of the liver and liver-brain axis dysfunction in Alzheimer's disease. Evidence has pointed to the liver as a target organ in Alzheimer's due to its role in regulating metabolism and supporting the immune system [54–56]. Researchers have proposed that impaired liver function due to chronic liver diseases and inflammation leads to an imbalance in peripheral Aβ clearance, exacerbating amyloid burden and Alzheimer's pathology [57, 58]. However, in our study, male 3xTg-AD mice with severe hepatic inflammation did not exhibit plaque pathology. This implies that the liver likely has a broader role outside of amyloid clearance alone in its contributions to Alzheimer's pathogenesis.

Heightened levels of CD45 + and F4/80 + cells have been described in the livers of 24-month-old male C57BL/6 mice [59] and Fischer rats [60]. While we did not observe evidence of increasing CD45 or F4/80 staining in our controls at up to 18-months of age (Fig. 3b-e), it is possible that there is a delayed or rapid onset of age-related hepatic inflammation in B6129 mice. Further, the hepatic inflammation observed in male 3xTg-AD mice could be the result of an accelerated aging phenotype in the male Alzheimer's disease trajectory. While limited studies have investigated the impact of aging on hepatic inflammation and function in humans, strong evidence supports the connection between liver and brain-related maladies, as non-alcoholic fatty liver disease has been linked to an increased risk of dementia [61]. A clinical study of over 450,000 participants [62] revealed that males were more likely to experience liver fibrosis and exhibited higher associations between liver fibrosis and most cognitive performance tests, suggesting that hepatic inflammation has a greater neurological impact in males than in females. However, the precise relationship between liver pathology, neuropathology, and neurodegeneration remains unclear.

To elucidate the temporal relationship between hepatic and neuroinflammation in the 3xTg-AD mouse model, we performed sex-specific longitudinal analyses of age and disease-related neural gene expression changes (Fig. 4). This study is one of the first to delineate sex-specific molecular timelines of disease progression in the 3xTg-AD model, revealing accelerated rates of neuroinflammation in male 3xTg-AD mice through the over-representation of immune-related processes beginning at 12-months-old in males and 18-months-old in females. These results were initially surprising, given the escalating presence of Alzheimer's neuropathology in female 3xTg-AD mice from 12-months of age onward, in addition to the commonly accepted paradigm that females develop stronger immune responses than males. However, age is a key variable that influences the strength and effectiveness of immune responses. Male and female immune responses change greatly over the life course [32]. Post-puberty and throughout the majority of adulthood, females exhibit heightened innate and adaptive immunity compared to males, resulting in 80% of autoimmune disease occurrence and greater vaccine efficacy in women. However, in old age, inflammation associated with innate immunity is heightened in males compared to females. The rate of "inflammaging" is also greater in men [33–35], driving a gap in male and female life expectancies. This process likely plays a key role in the pathogenesis of age-related diseases, including Alzheimer's [36].

A key contributor to the development and progression of inflammaging is the senescence associated secretory phenotype (SASP) – a damaging byproduct

of senescent cells [63], and a potential driver of Alzheimer's pathogenesis [64]. Cellular senescence is a tumor suppression mechanism which prevents the uncontrolled proliferation of old and injured cells. Despite the protective intent of this mechanism, senescent cells are accompanied by SASP which is comprised of secreted proteases and insoluble proteins, as well as soluble signaling factors such as interleukins, chemokines, and growth factors. Senescence is widely accepted as a major cause of age-related disease. The accumulation of senescent cells drives chronic immune induction, which in turn impairs the clearance of senescent cells, creating a detrimental cycle that fuels inflammaging [63]. We showed that aged 3xTg-AD male mice in particular, exhibit elevated plasma levels of known SASP factors [65, 66], including IL-12, IL-10, IL-6, CXCL2, CXCL1, and G-CSF (see Supplementary Fig. 1, Additional file 4). Together, our data in the liver, spleen, plasma, and brain clearly implicate chronic immune upregulation in Alzheimer's disease-associated mortality. Thus, we predict that biological aging and consequential age-associated inflammation are key drivers behind the sex differences observed in 3xTg-AD mice.

To further elucidate the impact of disease progression on the transcriptomic profiles of aged 3xTg-AD brains, we performed differential expression analysis with direct comparison to controls, which revealed a female-specific primary disease phenotype associated with impaired synaptic function and neurotransmitter signaling pathways (Fig. 5a, c). These results imply that 3xTg-AD females experience more neurodegeneration than males; therefore, the neuroinflammation observed in female and male 3xTg-AD brains may be the consequence of distinct forces. In Alzheimer's disease, neuroinflammation is primarily thought to be a consequence of a series of damage signals including trauma, oxidation, oligomers of Aβ and tau, and more [67]. Immune processes are triggered to maintain homeostasis and protect the neural environment. Eventually, however, neuroinflammation becomes chronic, initiating a cyclic cascade of glial priming, pro-inflammatory factor release, and neuronal damage [68]. Neuropathological and molecular changes associated with neuroinflammation in 3xTg-AD females align with this described pathogenic mechanism. Progressive plaque and tangle pathology were first observed in 3xTg-AD females at 12 months and 15 months of age respectively, subsequently followed by escalating neuroinflammation between 18 and 24 months of age (Figs. 2a-d and 4c). However, neuroinflammation in 3xTg-AD males does not follow this timeline, suggesting that an earlier trigger kicks off an unrelenting immune cascade, driven by earlier disease abnormalities as opposed to later stage disease pathology.

One key similarity between the sexes, and one of the most clearly perturbed biological pathways in our study, was an overactive complement system, a vital element of the immune system that enhances the opsonization of pathogens and initiates a series of inflammatory responses to help fight infection [51]. The primary action of the complement system is to enable the uptake and destruction of pathogens by phagocytic cells, which are microglia in the brain. In aged 3xTg-AD mice, the complement system had the greatest ratio of DEGs among top altered canonical pathways in both male and female brains (Fig. 5g). Upregulation of *C1q*, which is known to bind to Aβ peptides [69], NFT filaments [70], apoptotic cells and extracellular debris [71], indicated that the classical activation pathway was activated. Interestingly, 3xTg-AD males exhibited more extensive complement system overactivation than females, as differentially expressed complement genes were more statistically significant with greater log-fold changes.

Strong evidence has implicated the complement system in the pathogenesis of Alzheimer's disease [72–76], but questions remain regarding the impact of sex on complement activation and microglial phagocytosis. Several studies point to more potent and plentiful complement factors, and higher rates of microglial phagocytosis in males [77–80], while others find the opposite sex-difference in females [81–83]. Similar to other immune system studies previously described, age is likely a key variable between these experiments, which is especially difficult to capture in *in-vitro* studies, and strongly influences sex-specific results. Further, studies manipulating the complement system have yielded mixed results. The deficiency of complement factors such as C1q, C3, C3ar1, C5aR, and Cd59, has exacerbated neuropathology in some studies [84–86] and reduced neuropathology in others [87–89]. Additionally, multiple studies have shown that complement factor inhibition ameliorates synapse and neuron loss [90–93]. Determining how and when to modulate the complement cascade to prevent abnormal activation will be crucial, and more longitudinal studies will aid in identifying the appropriate and helpful window of treatment. Our transcriptomic results suggest that targeting C1q could serve as a targeted solution to both harness protective actions and dampen destructive actions of the complement system.

To explore further the primary drivers of differential gene expression in aged 3xTg-AD brains, we performed upstream regulator analyses. Female and male 3xTg-AD neural transcriptomes yielded distinct upstream regulator predictions. Differential gene expression was predicted to be most influenced by LPS, immunoglobulin, and interferon-gamma activation in male 3xTg-AD brains (Fig. 6c), as opposed to *MAPT*, beta-estradiol, and

APP in female 3xTg-AD brains (Fig. 6a). These results further reinforce that male 3xTg-AD mice experience an inflammatory manifestation of disease. Further comparison between the strength of upstream regulator predictions in males and females revealed that the other proinflammatory factors [94–96] most associated with inflammaging – IL-1B, IL-6, and TNFα – all have statistically greater predictions of activation in male 3xTg-AD brains, with z-scores three to 15-fold larger than that of females. We were surprised to discover that LPS, an outer-membrane component of gram-negative bacteria and an intense stimulator of the innate immune system, is the leading top predicted upstream regulator of gene expression changes in the male 3xTg-AD brain. Serum screening in sentinel mice confirmed the absence of any known pathogens (see Supplementary Table 1, Additional file 1 for list of tested agents). Therefore, an endogenous abnormality is triggering a pathogen-like response in 3xTg-AD males.

This finding complements the strong body of evidence that 3xTg-AD males exhibit a sex-dependent spontaneous autoimmune response. Marchese et al. showed that 3xTg-AD male mice exhibit elevated serum autoantibodies, reduced hematocrit, increased double-negative T splenocytes, splenomegaly, and hepatomegaly, which progress between 2 and 12 months of age [26]. Kapadia et al. further revealed that these manifestations of autoimmunity are exacerbated in 3xTg-AD males relative to females at 6 months of age [27]. An additional follow up study treated 3xTg-AD and WT mice with cyclophosphamide or a vehicle control, to examine the effects of general immunosuppression on autoimmune manifestations [28]. Chronic immunosuppression resulted in reduced hepatosplenomegaly, autoantibody levels, and regulatory T cell proportions relative to effector T cell populations. Our RNA-sequencing study provided evidence that the transcriptome of the aged 3xTg-AD male brain is primarily regulated by an endogenous immune response – potentially autoimmune in nature.

To broaden the translational impact of our work, we sought to verify the results obtained from our animal model in clinical data. We analyzed DEG data generated by The Mount Sinai/JJ Peters VA Medical Center NIH Brain and Tissue Repository, comparing the parahippocampal gyri of female and male Alzheimer's brains to age-matched controls [39]. We found overwhelming similarities between the mouse and human data. We again observed a female-specific primary disease phenotype associated with impaired synaptic function, implying advanced neurodegeneration in the female Alzheimer's parahippocampal gyrus (Fig. 5b). Additionally, the top altered canonical pathway in the male Alzheimer's parahippocampal gyrus was neutrophil extracellular trap signaling, an immune process activated by pathogens, antibodies, cytokines, and other physiological stimuli (Fig. 5f). In both the 3xTg-AD mouse model, and in humans with Alzheimer's, we see sex-specific disease phenotypes primarily driven by compromised neuronal function in females and aggravated immune response in males. Further, detailed gene expression analyses revealed significant upregulation of complement system genes in male and female Alzheimer's parahippocampal gyri (Fig. 5h). Both animal and human results suggest that sex may impact the extent of complement system activation, as males exhibited a heightened upregulation of complement system gene expression in the brain. Furthermore, the leading predicted upstream regulator of differential gene expression in the male Alzheimer's parahippocampal gyrus was LPS, precisely matching our observations in the male 3xTg-AD brain.

The infectious hypothesis proposes that a pathogen is the primary driver of Alzheimer's disease [97, 98]. Studies have linked oral bacteria [99], the gut microbiome [100, 101], herpesviruses [102], and other environmental pathogens with an increased risk of dementia. Theories regarding the involvement of Alzheimer's neuropathology in the infectious hypothesis differ. Plaques and tangles are posed to either associate with pathogens directly or develop as a result of infection-driven inflammation. Given that LPS was predicted as the leading upstream regulator in males of both species, our results suggest that females are less impacted by pathogens, an endogenous pathogen-like trigger, or an autoimmune response, and that males are more susceptible to an infectious or inflammatory mode of Alzheimer's initiation. Hence, we suggest that the male-biased immune manifestations of Alzheimer's disease resemble the downstream effects of LPS stimulation (Fig. 6e). We hypothesize that the mutations in *APP, MAPT,* and *PSEN1* genes, yield a compounding effect with age. The resulting biological changes initiate a neuroinflammatory response that mimics the effects of LPS stimulation, likely characterized by microglial activation. Pro-inflammatory factors, and well-known drivers of inflammaging, are activated including IL-1β, IL-6, TNFα, and IFNγ, in addition to the complement system. We hypothesize that persistent complement-mediated microglial phagocytosis clears and prevents the formation of plaques and tangles in the male 3xTg-AD brain, while the chronic inflammatory environment results in liver inflammation, spleen enlargement, and circulating inflammatory proteins in the bloodstream, driving increased mortality.

This hypothesis is substantiated by published literature revealing sex differences in microglial signature and response to complement receptor agonism. Hanamsager et al. [103] identified a microglia-specific gene expression

program in mice which enabled the generation of a microglial developmental index. This work showed that in response to LPS injection, male C57BL/6 microglia elicit an aged phenotype characterized by heightened upregulation of immune gene expression relative to female derived microglia. Additionally, healthy human male brains were found to exhibit "older" microglial signatures than age-matched female brains. Brains from individuals with Alzheimer's disease were also found to exhibit "older" microglial signatures than age-matched controls. While sex-specific analyses were not conducted with Alzheimer's data in this study, our results support the prediction that microglia from male Alzheimer's brains would exhibit the "oldest" reactive microglial signature.

Further, Stephen et al. [104] examined how sex and *APOE* genotype affect microglial interactions with plaques in the EFAD Alzheimer's mouse model. They discovered that microglial coverage of amyloid plaques is highest in male *APOE3* mice and reduced by female sex and *APOE4* genotype. Thus, female sex contributes to impaired microglial protective action in the Alzheimer's brain, supporting our hypothesis that males exhibit lower Aβ plaque burden as a result of exacerbated immune response. El Gaamouch et al. [86] treated 5xFAD mice with a VGF-derived peptide which activates complement C3a receptor-1 (C3aR1), predominantly expressed in the brain on microglia. Interestingly, treatment significantly reduced Aβ plaque load in males but not in females. This work provides additional evidence that the complement system regulates Alzheimer's neuropathology and suggests that either the male immune system is more effective at clearing and preventing protein aggregation, or that advanced pathological burden in the female brain reaches a point of no return. Our analyses of clinical Alzheimer's disease data confirm that widespread inflammation in 3xTg-AD males is not simply a consequence of transgenic mouse model development, and that further investigation into the mechanisms behind sex-specific immune responses in Alzheimer's disease is warranted.

Limitations

Sample size of the 3xTg-AD transgenic mouse model of Alzheimer's disease was small. In order to investigate the effects of sex, strain, and age, we experimentally examined nearly 30 sub cohorts of mice between the ages of 3- and 24-months-old, which made it particularly challenging to achieve larger sample sizes in each grouping, especially in older mice with higher rates of mortality. Despite constraints on sample size, our histology data established age and sex-specific effects of moderate and large size and our sequencing data revealed differentially expressed genes with a high degree of statistical significance. Our research could not be conducted with comparable longitudinal experimental design in humans. The 3xTg-AD mouse model contains three mutations associated with familial dementia (APP Swedish, MAPT P301L, and PSEN1 M146V), yet the vast majority of Alzheimer's disease cases manifest sporadically and are not associated with these specific mutations. However, our analyses of clinical data from patients with sporadic late onset Alzheimer's disease further validated the translational relevance of and lessened the limitations associated with the 3xTg-AD model in the context of this study.

Conclusions

In conclusion, our data demonstrate that chronic inflammation and complement activation are associated with increased mortality, suggesting that age-related changes in immune response act as a key contributor to sex differences in Alzheimer's disease trajectories. Current "disease- modifying" FDA-approved therapies for Alzheimer's are anti-amyloid antibody drugs, which successfully eliminate amyloid fibrils from the brain and produce an overall significant difference in performance on cognitive assessment scales [105]. However, despite reaching statistical significance, the clinical impact of treatment on individual patients and caregivers remains unclear [106]. Our study shows that destructive neuro- and systemic inflammation occurs without the presence of Aβ plaque pathology in the male 3xTg-AD mouse model, raising questions regarding the true impact of the protein in the progression of disease. Further, we demonstrate that males and females manifest distinct timelines of Alzheimer's disease progression and will require a personalized medicine approach to prevent and treat dementia most effectively. The data presented in this study provides evidence that aging affects the immune system of males and females differently. Sex-differences in inflammaging must be further studied in order to develop effective therapeutics that incorporate patient demographics and evolve past a one-size-fits-all approach to treating patients with Alzheimer's disease.

Abbreviations

Aβ	Amyloid Beta
AD	Alzheimer's disease
ANOVA	Analysis of Variance
CCL	CC chemokine ligand
CD45	Leukocyte common antigen
CT	Controls (human)
CXCL	CXC chemokine ligand
DEGs	Differentially Expressed Genes
EDTA	Edetic Acid
G-CSF	Granulocyte-Colony Stimulating Factor
GO	Gene Ontology
Ig	Immunoglobulin
IL	Interleukin
IPA	Ingenuity Pathway Analysis
LPS	Lipopolysaccharide

MSBB	Mount Sinai Brain Bank
NFTs	Neurofibrillary Tangles
ORA	Overrepresentation Analysis
PHG	Parahippocampal Gyrus
RNA-Seq	RNA Sequencing
SASP	Senescence Associated Secretory Phenotype
WT	Wildtype (B6129 mice)

Supplementary Information

The online version contains supplementary material available at https://doi.org/10.1186/s13195-024-01492-x.

Additional file 1: Supplementary Table 1. Serology testing agents. Bacteria and viruses tested in sentinel animal blood.

Additional file 2: Supplementary Table 2. Abnormalities observed during animal necropsy.

Additional file 3: Supplementary Table 3. Linear regression coefficients, effect sizes, and f-statistics.

Additional file 4: Supplementary Figure 1. 3xTg-AD males exhibit an age-dependent increase in circulating inflammatory proteins. Cytokine concentrations were measured in plasma from female and male, 3xTg-AD and WT mice, at ages 6-, 15-, 18-, 21-, and 24-months (oldest age dependent upon survival) (n = 3-6/sex + age + strain). Observed plasma concentrations of (A) IL-12 p40, (B) IL-10, (C) IL-6, (D) CCL4, (E) CXCL2, (F) CXCL1, (G) G-CSF, (H) CXCL5, (I) CXCL9, and (J) CXCL10. Data points considered out of range below were substituted with a 0, the minimum detectable value. Data were analyzed with a linear regression model (see extended results in Supplementary Table 3, Additional file 3). *P*-values less than 0.05 were considered statistically significant. Asterisks indicate significant differences between compared groups (* = $p < 0.05$, ** = $p \leq 0.01$, *** = $p \leq 0.001$, **** = $p \leq 0.0001$). Error bars represent mean with SD.

Additional file 5: Supplementary Figure 2. Exploratory analysis of complete RNA sequencing sample pool. (A) Hierarchical clustering based on Euclidian distance. Euclidian distance values for each sample compared to all other samples are plotted. Sample characteristics including sex, mouse strain, age, and sequencing batch are indicated. (B) Variance of top 10 principal components. (C) Principal component 1 plotted against principal component 2, showing complete sample clustering based on sex. (D) Principal component 3 plotted against principal component 2, showing no strong sample clustering based on sequencing batch.

Additional file 6: Supplementary Table 4. Genes differentially expressed in female and male, 3xTg-AD and WT mice between ages. Total RNA was isolated from the bulk brain tissue of female and male, 6–24-month-old (oldest age variable), 3xTg-AD and WT mice, and sequenced. Longitudinal differential expression analyses were performed, measuring differences in gene expression of subsequent ages compared to a baseline of 6-months-old (n = 3-4/sex+age+strain) with a negative binomial generalized linear model.

Additional file 7: Supplementary Table 5. Altered pathways between ages in 3xTg-AD and WT females. Altered biological pathways involving differentially expressed genes identified in female 3xTg-AD brains between various age groups were predicted using Enrichr.

Additional file 8: Supplementary Table 6. Altered pathways between ages in 3xTg-AD and WT males. Altered biological pathways involving differentially expressed genes identified in male 3xTg-AD brains between various age groups were predicted using Enrichr.

Additional file 9: Supplementary Figure 3. Longitudinal gene expression in control mice. Total RNA was isolated from the bulk brain tissue of female and male, 6–21-month-old, WT mice and sequenced. Longitudinal differential expression analyses were performed, measuring differences in gene expression of subsequent ages compared to a baseline of 6-months-old (n = 3-4/age). (A) Heatmap of genes with differential expression in WT females over the course of disease progression (padj < 0.05). Each column represents an individual animal, and age at time of collection is indicated by color. Samples range from 6-21 months of age. (B) Heatmap of genes with differential expression in WT males over the course of disease progression (padj < 0.05). Each column represents an individual animal, and age at time of collection is indicated by color. Samples range from 6-21 months of age. (C) Overrepresentation analysis of significant DEGs between various ages and a 6-month-old baseline. Affinity propagated, overrepresented GO biological processes are plotted for females in pink and males in blue. Data were analyzed by one-tailed Fisher's Exact test. *P*-values were adjusted for multiple comparisons via Benjamini-Hochberg correction. Number of DEGs indicates number of significant differentially expressed genes from dataset driving enrichment of biological processes.

Additional file 10: Supplementary Figure 4. Visualization of differential gene expression in 15–18-month-old mice. Differential expression analyses of RNA from bulk brain tissue were conducted between female and male 3xTg-AD and WT mice at 15–18 months of age. (A) Log2 fold change of each gene plotted against its adjusted *p*-value. Difference in gene expression between females. (B) Hierarchical clustering of all significant differentially expressed genes (padj < 0.05). 3xTg-AD female samples cluster separately from WT female samples. (C) Log2 fold change of each gene plotted against its adjusted *p*-value. Difference in gene expression between males. (D) Hierarchical clustering of all significant differentially expressed genes (padj < 0.05). 3xTg-AD male samples cluster separately from WT male samples.

Additional file 11: Supplementary Table 7. Genes differentially expressed in female and male, 15–18-month-old, 3xTg-AD mice compared to controls. Total RNA was isolated from the bulk brain tissue of 15–18- month-old, female and male, 3xTg-AD and WT mice, and sequenced. Differential expression analyses were performed between female 3xTg-AD and WT mice (n = 6 3xTg-AD, 6 WT) as well as between male 3xTg-AD and WT mice (n = 6 3xTg-AD, 6 WT) with a negative binomial generalized linear model.

Additional file 12: Supplementary Table 8. Altered pathways in female and male aged 3xTg-AD and post-mortem AD brains. Altered canonical pathways involving differentially expressed genes identified in 15-18-month-old 3xTg-AD brains and post-mortem AD PHG tissue were predicted using QIAGEN IPA.

Additional file 13: Supplementary Table 9. Predicted upstream regulators in female and male aged 3xTg-AD and post-mortem AD brains. Upstream regulators of differentially expressed genes identified in 15-18-month-old 3xTg-AD brains and post-mortem AD PHG tissue were predicted using QIAGEN IPA.

Acknowledgements

RNA sequencing was carried out in the Genomics and Molecular Biology Shared Resource (GMBSR) at Dartmouth which is supported by NCI Cancer Center Support Grant 5P30CA023108 and NIH S10 (1S10OD030242) awards. We especially thank Dr. Fred Kolling, PhD for his guidance and experimental support. The skills and tools necessary to conduct RNA sequencing data analyses were acquired through the Data Analytic Core of Geisel School of Medicine at Dartmouth's Center for Quantitative Biology which is supported through a grant from the National Institute of General Medical Sciences of the National Institutes of Health under award number P20GM130454. We thank Dr. Shannon Soucy, PhD for her instruction, advice, and technical support. The Center for Comparative Medicine and Research (CCMR) at Dartmouth maintained animal cages, monitored animal safety, provided animal handling trainings, and performed retro-orbital bleeds. We thank Kathryn Bennett and Stephen Gunn for their services and care. The Pathology Shared Resource at Dartmouth performed tissue processing, antibody staining, and slide imaging for all immunohistochemistry experiments. The Pathology Shared Resource is part of the Center for Clinical Genomics and Advanced Technology in the Department of Pathology and Laboratory Medicine at the Dartmouth Cancer Center and is supported by NCI Cancer Center Support Grant 5P30 CA023108-37. We thank Scott Palisoul for his technical services, antibody selection guidance, and protocol optimization feedback. Cytokine profiling experiments were carried out in DartLab, the Immune Monitoring and Flow Cytometry Shared Resource at the Norris Cotton Cancer Center at Dartmouth, with NCI Cancer Center Support Grant 5P30 CA023108-41. We thank Dr. Daniel Mielcarz, PhD and Andrew Calkins for their support and technical services. We

thank Drs. Ta Yuan Chang, PhD, Francesca Gilli, PhD, and Lucas Salas, MD, MPH, PhD for their expert guidance and manuscript review.
The data available in the AD Knowledge Portal would not be possible without the participation of research volunteers and the contribution of data by collaborating researchers. Data generation for The RNAseq Harmonization Study, which includes the data utilized in this work from the MSBB study, was supported by the following NIH grants: P30AG10161, P30AG72975, R01AG15819, R01AG17917, R01AG036836, U01AG46152, U01AG61356, U01AG046139, P50 AG016574, R01 AG032990, U01AG046139, R01AG018023, U01AG006576, U01AG006786, R01AG025711, R01AG017216, R01AG003949, R01NS080820, U24NS072026, P30AG19610, U01AG046170, RF1AG057440, and U24AG061340, and the Cure PSP, Mayo and Michael J Fox foundations, Arizona Department of Health Services and the Arizona Biomedical Research Commission. Data and analysis contributing investigators include Nilüfer Ertekin-Taner, Steven Younkin (Mayo Clinic, Jacksonville, FL), Todd Golde (University of Florida), Nathan Price (Institute for Systems Biology), David Bennett, Christopher Gaiteri (Rush University), Philip De Jager (Columbia University), Bin Zhang, Eric Schadt, Michelle Ehrlich, Vahram Haroutunian, Sam Gandy (Icahn School of Medicine at Mount Sinai), Koichi Iijima (National Center for Geriatrics and Gerontology, Japan), Scott Noggle (New York Stem Cell Foundation), Lara Mangravite (Sage Bionetworks). We thank the Mount Sinai/JJ Peters VA Medical Center NIH Brain and Tissue Repository.

Authors' contributions

AB contributed to study design, maintained the animal colony, was responsible for all aspects of data acquisition and analysis, and wrote the manuscript. CD contributed to study design and data acquisition by initiating animal colony breeding, animal colony maintenance, and biospecimen collection. ABS contributed to data acquisition and the development and execution of the immunohistochemistry quantification protocol, biospecimen collection and organization, and animal colony maintenance. EP contributed to data acquisition, biospecimen collection and animal colony maintenance. SW contributed to data acquisition and immunohistochemistry quantification. VT reviewed RNA-Seq data and analyses. GZ supervised immunohistochemistry work as well as reviewed and revised the manuscript. AG developed and supervised the study, as well as reviewed and revised the manuscript. All authors approved the final version of the manuscript.

Funding

Funds from the Dartmouth Health patient and family giving program supported the purchase and maintenance of the 3xTg-AD and WT mouse colonies for the first 2 years of this research.

Availability of data and materials

The RNA-seq dataset generated during the current study is deposited in NCBI's Gene Expression Omnibus and is accessible through GEO Series Accession Number GSE254970 (https://www.ncbi.nlm.nih.gov/geo/query/acc.cgi?acc=GSE254970). The results published here are in part based on data obtained from the AD Knowledge Portal (https://adknowledgeportal.org). Controlled data is accessible upon the submission and acceptance of a Data Use Certificate.

Declarations

Ethics approval and consent to participate

All applicable national and institutional guidelines for the care and use of animals were followed.

Consent for publication

Not applicable.

Competing interests

The authors declare no competing interests.

Author details

[1]Department of Neurology, Geisel School of Medicine, Dartmouth-Hitchcock Medical Center, Lebanon, NH, USA. [2]Integrative Neuroscience at Dartmouth, Dartmouth College, Hanover, NH, USA. [3]Department of Neurology, Dartmouth-Hitchcock Medical Center, Lebanon, NH, USA. [4]Dartmouth College, Hanover, NH, USA. [5]The Jackson Laboratory, Bar Harbor, ME, USA. [6]Neuroscience Program, Graduate School of Biomedical Sciences, Tufts University, Boston, MA, USA. [7]Department of Pathology, Geisel School of Medicine, Dartmouth-Hitchcock Medical Center, Lebanon, NH, USA.

Received: 5 February 2024 Accepted: 6 June 2024
Published online: 22 June 2024

References

1. Guo T, Zhang D, Zeng Y, Huang TY, Xu H, Zhao Y. Molecular and cellular mechanisms underlying the pathogenesis of Alzheimer's disease. Mol Neurodegener. 2020;15(1):1–37.
2. Serrano-Pozo A, Frosch MP, Masliah E, Hyman BT. Neuropathological alterations in Alzheimer disease. Cold Spring Harbor Perspect Med. 2011;1(1):a006189.
3. Dementia statistics. https://www.alzint.org/about/dementia-facts-figures/dementia-statistics/. Accessed 8 Jan 2024.
4. Armstrong RA. What causes Alzheimer's disease? Folia Neuropathol. 2013;51(3):169–88.
5. Ginter E, Simko V. Women live longer than men. Bratisl Lek Listy. 2013;114(2):45–9.
6. Yan BW, Arias E, Geller AC, Miller DR, Kochanek KD, Koh HK. Widening gender gap in life expectancy in the US, 2010–2021. JAMA Intern Med. 2023;184(1):108-10.
7. Stern Y, Tang M-X, Albert MS, Brandt J, Jacobs DM, Bell K, Marder K, Sano M, Devanand D, Albert SM. Predicting time to nursing home care and death in individuals with Alzheimer disease. JAMA. 1997;277(10):806–12.
8. Lapane K, Gambassi G, Landi F, Sgadari A, Mor V, Bernabei R. Gender differences in predictors of mortality in nursing home residents with AD. Neurology. 2001;56(5):650–4.
9. Haaksma ML, Eriksdotter M, Rizzuto D, Leoutsakos J-MS, Rikkert MGO, Melis RJ, Garcia-Ptacek S. Survival time tool to guide care planning in people with dementia. Neurology. 2020;94(5):e538–48.
10. Barnes LL, Wilson RS, Bienias JL, Schneider JA, Evans DA, Bennett DA. Sex differences in the clinical manifestations of Alzheimer disease pathology. Arch Gen Psychiatry. 2005;62(6):685–91.
11. Irvine K, Laws KR, Gale TM, Kondel TK. Greater cognitive deterioration in women than men with Alzheimer's disease: a meta analysis. J Clin Neuropsychol. 2012;34(9):989–98.
12. Holland D, Desikan RS, Dale AM, McEvoy LK. Higher rates of decline for women and apolipoprotein E ε4 carriers. AJNR Am J Neuroradiol. 2013;34(12):2287–93.
13. Oveisgharan S, Arvanitakis Z, Yu L, Farfel J, Schneider JA, Bennett DA. Sex differences in Alzheimer's disease and common neuropathologies of aging. Acta Neuropathol. 2018;136:887–900.
14. Dementia. https://www.who.int/news-room/fact-sheets/detail/dementia. Accessed 8 Jan 2024.
15. Oksuzyan A, Juel K, Vaupel JW, Christensen K. Men: good health and high mortality. Sex differences in health and aging. Aging Clin Exp Res. 2008;20:91–102.
16. Alberts SC, Archie EA, Gesquiere LR, et al. The Male-Female Health-Survival Paradox: A Comparative Perspective on Sex Differences in Aging and Mortality. In: Committee on Population; Division of Behavioral and Social Sciences and Education; National Research Council; Weinstein M, Lane MA, editors. Sociality, Hierarchy, Health: Comparative Biodemography: A Collection of Papers. Washington (DC): National Academies Press (US); 2014.
17. Oddo S, Caccamo A, Shepherd JD, Murphy MP, Golde TE, Kayed R, Metherate R, Mattson MP, Akbari Y, LaFerla FM. Triple-transgenic model of Alzheimer's disease with plaques and tangles: intracellular Aβ and synaptic dysfunction. Neuron. 2003;39(3):409–21.
18. Oddo S, Caccamo A, Kitazawa M, Tseng BP, LaFerla FM. Amyloid deposition precedes tangle formation in a triple transgenic model of Alzheimer's disease. Neurobiol Aging. 2003;24(8):1063–70.
19. Clinton LK, Billings LM, Green KN, Caccamo A, Ngo J, Oddo S, McGaugh JL, LaFerla FM. Age-dependent sexual dimorphism in cognition and stress response in the 3xTg-AD mice. Neurobiol Dis. 2007;28(1):76–82.
20. Giménez-Llort L, Arranz L, Maté I, De la Fuente M. Gender-specific neuroimmunoendocrine aging in a triple-transgenic 3× Tg-AD

mouse model for Alzheimer's disease and its relation with longevity. Neuroimmunomodulation. 2008;15(4–6):331–43.
21. Kane AE, Shin S, Wong AA, Fertan E, Faustova NS, Howlett SE, Brown RE. Sex differences in healthspan predict lifespan in the 3xTg-AD mouse model of Alzheimer's disease. Front Aging Neurosci. 2018;10:172.
22. Belfiore R, Rodin A, Ferreira E, Velazquez R, Branca C, Caccamo A, Oddo S. Temporal and regional progression of Alzheimer's disease-like pathology in 3xTg-AD mice. Aging Cell. 2019;18(1):e12873.
23. Carroll JC, Rosario ER, Kreimer S, Villamagna A, Gentzschein E, Stanczyk FZ, Pike CJ. Sex differences in β-amyloid accumulation in 3xTg-AD mice: role of neonatal sex steroid hormone exposure. Brain Res. 2010;1366:233–45.
24. Hirata-Fukae C, Li H-F, Hoe H-S, Gray AJ, Minami SS, Hamada K, Niikura T, Hua F, Tsukagoshi-Nagai H, Horikoshi-Sakuraba Y. Females exhibit more extensive amyloid, but not tau, pathology in an Alzheimer transgenic model. Brain Res. 2008;1216:92–103.
25. B6;129-Tg(APPSwe,tauP301L)1Lfa *Psen1*^{tm1Mpm}/Mmjax. https://www.jax.org/strain/004807. Accessed 8 Jan 2024.
26. Marchese M, Cowan D, Head E, Ma D, Karimi K, Ashthorpe V, Kapadia M, Zhao H, Davis P, Sakic B. Autoimmune manifestations in the 3xTg-AD model of Alzheimer's disease. J Alzheimer's Dis. 2014;39(1):191–210.
27. Kapadia M, Mian MF, Michalski B, Azam AB, Ma D, Salwierz P, Christopher A, Rosa E, Zovkic IB, Forsythe P. Sex-dependent differences in spontaneous autoimmunity in adult 3xTg-AD mice. J Alzheimer's Dis. 2018;63(3):1191–205.
28. Kapadia M, Mian MF, Ma D, Hutton CP, Azam A, Narkaj K, Cao C, Brown B, Michalski B, Morgan D, et al. Differential effects of chronic immunosuppression on behavioral, epigenetic, and Alzheimer's disease-associated markers in 3xTg-AD mice. Alzheimers Res Ther. 2021;13(1):30.
29. Catorce MN, Acero G, Gevorkian G. Age-and sex-dependent alterations in the peripheral immune system in the 3xTg-AD mouse model of Alzheimer's disease: Increased proportion of CD3+ CD4-CD8-double-negative T cells in the blood. J Neuroimmunol. 2021;360:577720.
30. St-Amour I, Bosoi CR, Paré I, Ignatius Arokia Doss PM, Rangachari M, Hébert SS, Bazin R, Calon F. Peripheral adaptive immunity of the triple transgenic mouse model of Alzheimer's disease. J Neuroinflammation. 2019;16:1–12.
31. Franceschi C, Bonafè M, Valensin S, Olivieri F, De Luca M, Ottaviani E, De Benedictis G. Inflamm-aging: an evolutionary perspective on immunosenescence. Ann NY Acad Sci. 2000;908(1):244–54.
32. Klein SL, Flanagan KL. Sex differences in immune responses. Nat Rev Immunol. 2016;16(10):626–38.
33. Gubbels Bupp MR, Potluri T, Fink AL, Klein SL. The confluence of sex hormones and aging on immunity. Front Immunol. 2018;9:1269.
34. Bonafè M, Olivieri F, Cavallone L, Giovagnetti S, Marchegiani F, Cardelli M, Pieri C, Marra M, Antonicelli R, Lisa R. A gender–dependent genetic predisposition to produce high levels of IL-6 is detrimental for longevity. Eur J Immunol. 2001;31(8):2357–61.
35. Bonafè M, Prattichizzo F, Giuliani A, Storci G, Sabbatinelli J, Olivieri F. Inflamm-aging: why older men are the most susceptible to SARS-CoV-2 complicated outcomes. Cytokine Growth Factor Rev. 2020;53:33–7.
36. Giunta B, Fernandez F, Nikolic WV, Obregon D, Rrapo E, Town T, Tan J. Inflammaging as a prodrome to Alzheimer's disease. J Neuroinflammation. 2008;5(1):1–15.
37. Zhang Y, Parmigiani G, Johnson WE. ComBat-seq: batch effect adjustment for RNA-seq count data. Nar Genom Bioinform. 2020;2(3):lqaa078.
38. Love MI, Huber W, Anders S. Moderated estimation of fold change and dispersion for RNA-seq data with DESeq2. Genome Biol. 2014;15(12):1–21.
39. Wang M, Beckmann ND, Roussos P, Wang E, Zhou X, Wang Q, Ming C, Neff R, Ma W, Fullard JF, et al. The Mount Sinai cohort of large-scale genomic, transcriptomic and proteomic data in Alzheimer's disease. Sci Data. 2018;5(1):180185.
40. Krämer A, Green J, Pollard J Jr, Tugendreich S. Causal analysis approaches in ingenuity pathway analysis. Bioinform. 2014;30(4):523–30.
41. Chen EY, Tan CM, Kou Y, Duan Q, Wang Z, Meirelles GV, Clark NR, Ma'ayan A. Enrichr: interactive and collaborative HTML5 gene list enrichment analysis tool. BMC Bioinform. 2013;14(1):1–14.
42. Zhang B, Kirov S, Snoddy J. WebGestalt: an integrated system for exploring gene sets in various biological contexts. Nucleic Acids Res. 2005;33(suppl_2):W741–8.
43. Kozin SA, Kechko OI, Adzhubei AA, Makarov AA, Mitkevich VA. Switching on/off amyloid plaque formation in transgenic animal models of Alzheimer's disease. Int J Mol Sci. 2023;25(1):72.
44. Vickers JC, Morrison JH, Friedrich V, Elder G, Perl DP, Katz RN, Lazzarini RA. Age-associated and cell-type-specific neurofibrillary pathology in transgenic mice expressing the human midsized neurofilament subunit. J Neurosci. 1994;14(9):5603–12.
45. Games D, Adams D, Alessandrini R, Barbour R, Borthelette P, Blackwell C, Carr T, Clemens J, Donaldson T, Gillespie F. Alzheimer-type neuropathology in transgenic mice overexpressing V717F β-amyloid precursor protein. Nat. 1995;373(6514):523–7.
46. Hermida MdE-R, De Melo CVB, Lima IDS, Oliveira GGDS, Dos-Santos WL. Histological disorganization of spleen compartments and severe visceral leishmaniasis. Front Cell Infect. 2018;8:394.
47. Nakano A, Harada T, Morikawa S, Kato Y. Expression of leukocyte common antigen (CD45) on various human leukemia/lymphoma cell lines. Pathol Int. 1990;40(2):107–15.
48. Lifespan as a Biomarker. https://www.jax.org/research-and-faculty/research-labs/the-harrison-lab/gerontology/life-span-as-a-biomarker. Accessed 8 Jan 2024.
49. Dutta S, Sengupta P. Men and mice: relating their ages. Life Sci. 2016;152:244–8.
50. Neff RA, Wang M, Vatansever S, Guo L, Ming C, Wang Q, Wang E, Horgusluoglu-Moloch E, Song W-M, Li A. Molecular subtyping of Alzheimer's disease using RNA sequencing data reveals novel mechanisms and targets. Sci Adv. 2021;7(2):eabb5398.
51. Dunkelberger JR, Song W-C. Complement and its role in innate and adaptive immune responses. Cell Res. 2010;20(1):34–50.
52. Fraile-Ramos J, Garrit A, Reig-Vilallonga J, Giménez-Llort L. Hepatic oxi-inflammation and neophobia as potential liver-brain axis targets for Alzheimer's disease and aging, with strong sensitivity to sex, isolation, and obesity. Cells. 2023;12(11):1517.
53. Chapman J, Goyal A, Azevedo AM. Splenomegaly. 2017.
54. Lam V, Takechi R, Hackett MJ, Francis R, Bynevelt M, Celliers LM, Nesbit M, Mamsa S, Arfuso F, Das S. Synthesis of human amyloid restricted to liver results in an Alzheimer disease–like neurodegenerative phenotype. PLoS Biol. 2021;19(9):e3001358.
55. Kim D-G, Krenz A, Toussaint LE, Maurer KJ, Robinson S-A, Yan A, Torres L, Bynoe MS. Non-alcoholic fatty liver disease induces signs of Alzheimer's disease (AD) in wild-type mice and accelerates pathological signs of AD in an AD model. J Neuroinflammation. 2016;13:1–18.
56. Nho K, Kueider-Paisley A, Ahmad S, MahmoudianDehkordi S, Arnold M, Risacher SL, Louie G, Blach C, Baillie R, Han X. Association of altered liver enzymes with Alzheimer disease diagnosis, cognition, neuroimaging measures, and cerebrospinal fluid biomarkers. JAMA Netw Open. 2019;2(7):e197978.
57. Estrada LD, Ahumada P, Cabrera D, Arab JP. Liver dysfunction as a novel player in Alzheimer's progression: looking outside the brain. Front Aging Neurosci. 2019;11:174.
58. Huang Z, Lin HW, Zhang Q, Zong X. Targeting Alzheimer's disease: the critical crosstalk between the liver and brain. Nutrients. 2022;14(20):4298.
59. Mohammed S, Thadathil N, Selvarani R, Nicklas EH, Wang D, Miller BF, Richardson A, Deepa SS. Necroptosis contributes to chronic inflammation and fibrosis in aging liver. Aging Cell. 2021;20(12):e13512.
60. Hilmer SN, Cogger VC, Couteur DGL. Basal activity of Kupffer cells increases with old age. J Gerontol A Biol Sci Med Sci. 2007;62(9):973–8.
61. Shang Y, Widman L, Hagström H. Nonalcoholic fatty liver disease and risk of dementia: a population-based cohort study. Neurology. 2022;99(6):e574–82.
62. Jiang R, Wu J, Rosenblatt M, Dai W, Rodriguez RX, Sui J, Qi S, Liang Q, Xu B, Meng Q, Calhoun VD, Scheinost D. Elevated C-reactive protein mediates the liver-brain axis: a preliminary study. EBioMedicine. 2023;93:104679.
63. Olivieri F, Prattichizzo F, Grillari J, Balistreri CR. Cellular senescence and inflammaging in age-related diseases. Mediators Inflamm. 2018;2018:9076485.

64. Zhang P, Kishimoto Y, Grammatikakis I, Gottimukkala K, Cutler RG, Zhang S, Abdelmohsen K, Bohr VA, Misra Sen J, Gorospe M. Senolytic therapy alleviates Aβ-associated oligodendrocyte progenitor cell senescence and cognitive deficits in an Alzheimer's disease model. Nat Neurosci. 2019;22(5):719–28.
65. Maciel-Barón L, Morales-Rosales S, Aquino-Cruz A, Triana-Martínez F, Galván-Arzate S, Luna-López A, González-Puertos V, López-Díazguerrero N, Torres C, Königsberg M. Senescence associated secretory phenotype profile from primary lung mice fibroblasts depends on the senescence induction stimuli. Age. 2016;38:1–14.
66. Xu M, Tchkonia T, Ding H, Ogrodnik M, Lubbers ER, Pirtskhalava T, White TA, Johnson KO, Stout MB, Mezera V. JAK inhibition alleviates the cellular senescence-associated secretory phenotype and frailty in old age. Proct Natl Acad Sci USA. 2015;112(46):E6301–10.
67. Morales I, Guzmán-Martínez L, Cerda-Troncoso C, Farías GA, Maccioni RB. Neuroinflammation in the pathogenesis of Alzheimer's disease. A rational framework for the search of novel therapeutic approaches. Front Cell Neurosci. 2014;8:112.
68. Calsolaro V, Edison P. Neuroinflammation in Alzheimer's disease: current evidence and future directions. Alzheimer's Dement. 2016;12(6):719–32.
69. Jiang H, Burdick D, Glabe CG, Cotman CW, Tenner AJ. beta-Amyloid activates complement by binding to a specific region of the collagen-like domain of the C1q A chain. J Immunol (Baltimore, Md: 1950). 1994;152(10):5050–9.
70. Shen Y, Lue L-F, Yang L-B, Roher A, Kuo Y-M, Strohmeyer R, Goux WJ, Lee V, Johnson GV, Webster SD. Complement activation by neurofibrillary tangles in Alzheimer's disease. Neurosci Lett. 2001;305(3):165–8.
71. Nauta AJ, Trouw LA, Daha MR, Tijsma O, Nieuwland R, Schwaeble WJ, Gingras AR, Mantovani A, Hack EC, Roos A. Direct binding of C1q to apoptotic cells and cell blebs induces complement activation. Eur J Immunol. 2002;32(6):1726–36.
72. Eikelenboom P, Stam F. An immunohistochemical study on cerebral vascular and senile plaque amyloid in Alzheimer's dementia. Virchows Arch B. 1984;47:17–25.
73. Walker DG, McGeer PL. Complement gene expression in human brain: comparison between normal and Alzheimer disease cases. Brain Res Mol Brain Res. 1992;14(1–2):109–16.
74. Stoltzner SE, Grenfell TJ, Mori C, Wisniewski KE, Wisniewski TM, Selkoe DJ, Lemere CA. Temporal accrual of complement proteins in amyloid plaques in Down's syndrome with Alzheimer's disease. Am J Pathol. 2000;156(2):489–99.
75. Lambracht-Washington D, Fu M, Manouchehri N, Hynan LS, Stuve O, Rosenberg RN. Glial cell transcriptome analyses in 3xTg-AD mice: effects of aging, disease progression, and anti-Aβ immunotherapy. Aging Brain. 2023;3:100066.
76. Morgan BP. Complement in the pathogenesis of Alzheimer's disease. Springer Semin Immunopathol. 2018;40(1):113–24.
77. Kamitaki N, Sekar A, Handsaker RE, De Rivera H, Tooley K, Morris DL, Taylor KE, Whelan CW, Tombleson P, Loohuis LMO. Complement genes contribute sex-biased vulnerability in diverse disorders. Nature. 2020;582(7813):577–81.
78. Poppelaars F, Mollnes TE, Tedesco F, Wuerzner R, Trouw LA, Truedsson L, Daha MR, Roos A, Seelen MA. Age and sex-associated changes of complement activity and complement levels in a healthy Caucasian population. Front Immunol. 2018;9:2664.
79. Guillot-Sestier M-V, Araiz AR, Mela V, Gaban AS, O'Neill E, Joshi L, Chouchani ET, Mills EL, Lynch MA. Microglial metabolism is a pivotal factor in sexual dimorphism in Alzheimer's disease. Commun Biol. 2021;4(1):711.
80. Yanguas-Casás N, Crespo-Castrillo A, Arevalo MA, Garcia-Segura LM. Aging and sex: impact on microglia phagocytosis. Aging Cell. 2020;19(8):e13182.
81. Yang H, Oh C-K, Amal H, Wishnok JS, Lewis S, Schahrer E, Trudler D, Nakamura T, Tannenbaum SR, Lipton SA. Mechanistic insight into female predominance in Alzheimer's disease based on aberrant protein S-nitrosylation of C3. Sci Adv. 2022;8(50):eade0764.
82. Mangold CA, Wronowski B, Du M, Masser DR, Hadad N, Bixler GV, Brucklacher RM, Ford MM, Sonntag WE, Freeman WM. Sexually divergent induction of microglial-associated neuroinflammation with hippocampal aging. J Neuroinflammation. 2017;14:1–19.
83. Nelson LH, Warden S, Lenz KM. Sex differences in microglial phagocytosis in the neonatal hippocampus. Brain Behav Immun. 2017;64:11–22.
84. Maier M, Peng Y, Jiang L, Seabrook TJ, Carroll MC, Lemere CA. Complement C3 deficiency leads to accelerated amyloid β plaque deposition and neurodegeneration and modulation of the microglia/macrophage phenotype in amyloid precursor protein transgenic mice. J Neurosci. 2008;28(25):6333–41.
85. Wyss-Coray T, Yan F, Lin AH-T, Lambris JD, Alexander JJ, Quigg RJ, Masliah E. Prominent neurodegeneration and increased plaque formation in complement-inhibited Alzheimer's mice. Proc Natl Acad Sci USA. 2002;99(16):10837–42.
86. El Gaamouch F, Audrain M, Lin W-J, Beckmann N, Jiang C, Hariharan S, Heeger PS, Schadt EE, Gandy S, Ehrlich ME. VGF-derived peptide TLQP-21 modulates microglial function through C3aR1 signaling pathways and reduces neuropathology in 5xFAD mice. Mol Neurodegener. 2020;15(1):1–19.
87. Shi Q, Chowdhury S, Ma R, Le KX, Hong S, Caldarone BJ, Stevens B, Lemere CA. Complement C3 deficiency protects against neurodegeneration in aged plaque-rich APP/PS1 mice. Sci Transl Med. 2017;9(392):eaaf6295.
88. Czirr E, Castello NA, Mosher KI, Castellano JM, Hinkson IV, Lucin KM, Baeza-Raja B, Ryu JK, Li L, Farina SN. Microglial complement receptor 3 regulates brain Aβ levels through secreted proteolytic activity. J Exp Med. 2017;214(4):1081–92.
89. Fonseca MI, Ager RR, Chu S-H, Yazan O, Sanderson SD, LaFerla FM, Taylor SM, Woodruff TM, Tenner AJ. Treatment with a C5aR antagonist decreases pathology and enhances behavioral performance in murine models of Alzheimer's disease. J Immunol Res. 2009;183(2):1375–83.
90. Carpanini SM, Torvell M, Bevan RJ, Byrne RA, Daskoulidou N, Saito T, Saido TC, Taylor PR, Hughes TR, Zelek WM. Terminal complement pathway activation drives synaptic loss in Alzheimer's disease models. Acta Neuropathol Commun. 2022;10(1):1–16.
91. Britschgi M, Takeda-Uchimura Y, Rockenstein E, Johns H, Masliah E, Wyss-Coray T. Deficiency of terminal complement pathway inhibitor promotes neuronal tau pathology and degeneration in mice. J Neuroinflammation. 2012;9(1):1–6.
92. Fonseca MI, Zhou J, Botto M, Tenner AJ. Absence of C1q leads to less neuropathology in transgenic mouse models of Alzheimer's disease. J Neurosci. 2004;24(29):6457–65.
93. Hong S, Beja-Glasser VF, Nfonoyim BM, Frouin A, Li S, Ramakrishnan S, Merry KM, Shi Q, Rosenthal A, Barres BA. Complement and microglia mediate early synapse loss in Alzheimer mouse models. Science. 2016;352(6286):712–6.
94. Ferrucci L, Fabbri E. Inflammageing: chronic inflammation in ageing, cardiovascular disease, and frailty. Nat Rev Cardiol. 2018;15(9):505–22.
95. Cesari M, Penninx BW, Pahor M, Lauretani F, Corsi AM, Williams GR, Guralnik JM, Ferrucci L. Inflammatory markers and physical performance in older persons: the InCHIANTI study. J Gerontol A Biol Sci Med Sci. 2004;59(3):M242–8.
96. Bruunsgaard H, Andersen-Ranberg K, Hjelmborg JVB, Pedersen BK, Jeune B. Elevated levels of tumor necrosis factor alpha and mortality in centenarians. Am J Med. 2003;115(4):278–83.
97. Sochocka M, Zwolinska K, Leszek J. The infectious etiology of Alzheimer's disease. Curr Neuropharmacol. 2017;15(7):996–1009.
98. Seaks CE, Wilcock DM. Infectious hypothesis of Alzheimer disease. PLoS Pathog. 2020;16(11):e1008596.
99. Dominy SS, Lynch C, Ermini F, Benedyk M, Marczyk A, Konradi A, Nguyen M, Haditsch U, Raha D, Griffin C. Porphyromonas gingivalis in Alzheimer's disease brains: evidence for disease causation and treatment with small-molecule inhibitors. Sci Adv. 2019;5(1):eaau3333.
100. Chen C, Liao J, Xia Y, Liu X, Jones R, Haran J, McCormick B, Sampson TR, Alam A, Ye K. Gut microbiota regulate Alzheimer's disease pathologies and cognitive disorders via PUFA-associated neuroinflammation. Gut. 2022;71(11):2233–52.
101. Kesika P, Suganthy N, Sivamaruthi BS, Chaiyasut C. Role of gut-brain axis, gut microbial composition, and probiotic intervention in Alzheimer's disease. Life Sci. 2021;264:118627.
102. Huang S-Y, Yang Y-X, Kuo K, Li H-Q, Shen X-N, Chen S-D, Cui M, Tan L, Dong Q, Yu J-T. Herpesvirus infections and Alzheimer's disease: a Mendelian randomization study. Alzheimers Res Ther. 2021;13:1–8.
103. Hanamsagar R, Alter MD, Block CS, Sullivan H, Bolton JL, Bilbo SD. Generation of a microglial developmental index in mice and in humans

reveals a sex difference in maturation and immune reactivity. Glia. 2017;65(9):1504–20.
104. Stephen TL, Cacciottolo M, Balu D, Morgan TE, LaDu MJ, Finch CE, Pike CJ. APOE genotype and sex affect microglial interactions with plaques in Alzheimer's disease mice. Acta Neuropathol Commun. 2019;7(1):82.
105. Van Dyck CH, Swanson CJ, Aisen P, Bateman RJ, Chen C, Gee M, et al. Lecanemab in early Alzheimer's disease. New Eng J Med. 2023;388(1):9–21.
106. Lin GA, Whittington MD, Wright A, Agboola F, Herron-Smith S, Pearson SD, Rind DM. Beta-amyloid antibodies for early Alzheimer's disease: effectiveness and value; evidence report. Institute for Clinical and Economic Review; 2023. https://icer.org/assessment/alzheimers-disease-2022/#timeline.

Publisher's Note